



Discovery of novel FGF trap small molecules endowed with anti-myeloma activity

Sara Taranto^{a,b,1}, Riccardo Castelli^{c,1}, Giuseppe Marseglia^c, Laura Scalvini^c, Federica Vacondio^c, Alessandra Gianoncelli^a, Giovanni Ribaudo^a, Jessica Faletti^a, Giorgia Gazzaroli^a, Edoardo Rocca^c, Roberto Ronca^a, Marco Rusnati^a, Antonio Sacco^b, Aldo Maria Roccaro^b, Marco Presta^a, Marco Mor^c, Arianna Giacomini^{a,*},², Silvia Rivara^{c,*},²

^a Department of Molecular and Translational Medicine, University of Brescia, Brescia, Italy

^b Clinical Trial Center, Translational Research and Phase I Unit, ASST Spedali Civili di Brescia, Brescia, Italy

^c Department of Food and Drug, University of Parma, Parma, Italy

ARTICLE INFO

Keywords:

FGF trap

FGFR

NSC12

multiple myeloma

ABSTRACT

Fibroblast growth factors (FGFs) act as proangiogenic and mitogenic cytokines in several cancers, including multiple myeloma (MM). Indeed, corrupted FGF autocrine and paracrine secretion induces an aberrant activation of the FGF receptor (FGFR) signaling sustaining cancer cell spreading and resistance to pharmacological treatments. Thus, FGF traps may represent a promising anti-cancer strategy to hamper the ligand-dependent activation of the FGF/FGFR system. We previously identified NSC12 as the first orally available small molecule FGF trap able to inhibit the growth and progression of several FGF-dependent tumor models. NSC12 is a pregnenolone derivative carrying a 1,1-bis-trifluoromethyl-1,3-propanediol chain in position 17 of the steroid nucleus. Investigation of structure-activity relationships (SARs) provided more potent and specific NSC12 steroid derivatives and highlighted that the C17-side chain is pivotal for the FGF trap activity. Here, a scaffold hopping approach allowed to obtain two FGF trap compounds (**22** and **57**) devoid of the steroid nucleus and able to efficiently bind FGF2 and to inhibit FGFR activation in MM cells. Accordingly, these compounds exert a potent anti-tumor activity on MM cell lines both *in vitro* and *in vivo* and on MM patient-derived primary cells, strongly affecting the survival of both proteasome-inhibitor sensitive and resistant MM cells. These results propose a new therapeutic option for relapsed/refractory MM patients and set the bases for the development of novel FGF traps prone to chemical diversification to be used in the clinic for the treatment of those tumors in which the FGF/FGFR system plays a pivotal role, including MM.

1. Introduction

The system composed of fibroblast growth factors (FGFs) and their receptors plays a fundamental role in several developmental and physiological processes spanning from embryonal development and angiogenesis to tissue repair, wound healing and endocrine signaling [1]. The FGF family includes 18 secreted members and 4 intracellular FGF

homologous factors. The secreted members are grouped into six sub-families based on phylogenetic analysis and sequence homology. FGF1/2, FGF4/5/6, FGF3/7/10/22, FGF8/17/18, and FGF9/16/20 subfamilies act as “canonical” FGFs. Canonical FGFs bind and activate tyrosine kinase (TK) FGF receptors (FGFRs), triggering intracellular signaling cascades that mediate their biological activity [2]. On the cell surface, the interaction between FGF and FGFR is stabilized by heparan

Abbreviations: BPMD, binding pose metadynamics; BTZ, bortezomib; DCM, dichloromethane; DMAP, 4-dimethylaminopyridine; DMF, dimethylformamide; EDCl, 1-ethyl-3-(3-dimethylaminopropyl)carbodiimide; FBS, fetal bovine serum; FGF, fibroblast growth factor; FGFR, fibroblast growth factor receptor; H-ESI, heated electrospray ionization; HFA, hexafluoroacetone; HSPG, heparan sulfate proteoglycans; LiHMDS, lithium hexamethyldisilylamide; MM, multiple myeloma; PBS, phosphate buffered saline; RMSD, root-mean-square deviation; TBAF, Tetra-n-butylammonium fluoride; THF, tetrahydrofuran.

* Corresponding authors.

E-mail addresses: arianna.giacomini@unibs.it (A. Giacomini), silvia.rivara@unipr.it (S. Rivara).

¹ ST and RC share first authorship.

² AG and SR share last authorship.

<https://doi.org/10.1016/j.phrs.2024.107291>

Received 20 December 2023; Received in revised form 14 June 2024; Accepted 2 July 2024

Available online 3 July 2024

1043-6618/© 2024 The Author(s). Published by Elsevier Ltd. This is an open access article under the CC BY-NC-ND license (<http://creativecommons.org/licenses/by-nc-nd/4.0/>).

sulfate proteoglycans (HSPGs), leading to the formation of HSPG/FGF/FGFR ternary complexes that are essential for signal transduction [2].

Dysregulation of FGF/FGFR axis has been found to affect human health, sustaining the onset and progression of different pathologies. In particular, FGFR signaling has been involved in the onset and progression of cancer, sustaining cell proliferation, angiogenesis and anti-apoptotic effects [3]. Several dysfunctions have been shown to promote the hyperactivation of the FGF/FGFR system and abnormal cell signaling. These alterations are mainly related to FGFR aberrations due to chromosomal rearrangements and oncogenic fusions, gene amplification, and activating mutations that lead to ligand-independent receptor activation [4]. On the other hand, other mechanisms, such as corrupted FGF autocrine and paracrine signaling and FGFR interaction with noncanonical signaling partners, can affect receptor activity and sustain cancer cell invasiveness, metastatic potential, and resistance to pharmacological treatments [5].

The pharmacological approach based on FGF/FGFR inhibitors has emerged as a successful strategy for the effective treatment of cancer [6]. Inhibitors with different composition and mechanism are currently available. They comprise proteins, e.g., monoclonal antibodies and soluble decoy receptors, oligo- and polysaccharides, and small molecules. Within the latter group, FGFR TK inhibitors are the most advanced compounds, with drugs already approved for cancer treatment and others in advanced clinical trials [7]. Unfortunately, treatment with FGFR TK inhibitors has been associated with side effects, including hyperphosphatemia, and with occurrence of resistance that can be driven by several mechanisms comprising mutation of FGFR amino acid residues that abolishes drug activity and activation of other TK receptors. In this context, the development of agents that can avoid or overcome these limitations is currently actively pursued.

FGF traps represent an alternative strategy to hamper the ligand-dependent activation of the FGF/FGFR system by binding FGFs, thus preventing interaction with receptors expressed on plasma membranes [8]. Different types of FGF traps have been developed. They mimic heparan sulfate chains of HSPGs, involved in the formation of the functional heterotrimeric structure with FGF and FGFR, or act as decoy receptors built from truncated FGFR variants. FP-1039, consisting of the extracellular domain of FGFR1 fused with the Fc region of IgG1, was evaluated in a phase I clinical trial and patients showed no alteration of calcium and phosphate serum levels [9]. Another effective class of FGF traps was developed starting from the observation that pentraxin-3 (PTX3) is able to bind FGFs through its terminal amino portion [10]. A screening campaign based on a pharmacophore model built on the FGF-binding portion of PTX3 led to the identification of NSC12, a pregnenolone derivative carrying a 1,1-bis-trifluoromethyl-1,3-propanediol chain in position 17 of the steroid nucleus (1 in Fig. 1). NSC12 (1) was characterized as a multi-FGF trap able to inhibit the formation of the bioactive HSPG/FGF/FGFR ternary complex [11,12]. This compound inhibited the proliferation of several FGF-dependent cancer cell lines *in vitro*, and *in vivo* resulted to be orally available and able to reduce tumor growth, angiogenesis, and metastasis in various murine and human tumor models [11,12].

Investigation of structure-activity relationships (SARs) provided more potent NSC12 (1) derivatives through modulation of the

substituent in position 3, while attempts to replace the C17-side chain led to a decrease of activity. Structural optimization afforded compound 2 (Fig. 1), the pregnane 3-keto analog of compound 1, which exerted antiproliferative activity on several multiple myeloma (MM) cell lines and antitumor activity in a KMS-11 cell xenograft murine model of multiple myeloma (MM), producing a greater reduction of tumor growth than compound 1 [13].

The intrinsic difficulties in the modification and functionalization of the steroid nucleus of FGF traps 1 and 2 allowed a limited exploration of SARs. Therefore, to prospectively allow a wider investigation of the structural requirements for FGF binding and FGF/FGFR system signaling inactivation, a scaffold hopping approach was applied to obtain compounds devoid of the steroid nucleus. To this aim, various bioisosteric replacements were evaluated, to identify new scaffolds that could maintain the biological activity of parent steroid derivatives, while being more easily synthesized and more prone to chemical diversification.

We report here the first non-steroidal NSC12 derivatives able to efficiently bind FGF2 and to inhibit FGFR phosphorylation and endowed with antitumor activity on MM cell lines both *in vitro* and *in vivo* and on MM patient-derived primary cells.

2. Chemistry

The replacement of the steroidal portion of NSC12 (1) and 2, while retaining the *bis*-trifluoromethyl-1,3-propanediol chain, featured a common synthetic strategy centered around the aldol-type condensation of an aryl-methyl ketone with hexafluoroacetone (HFA), followed by reduction of the β -hydroxy ketone thus obtained (Scheme 1) [12,13].

The *para*-biphenyl functionalized compounds were prepared as depicted in Scheme 2. Suzuki-Miyaura cross coupling between ethyl-4-iodobenzoate and either 4- or 3-acetylphenylboronic acid furnished *para*-biphenyl methyl ketones 3 and 8, respectively [14,15]. These were subjected to condensation with HFA at low temperatures to give ketones 4 and 9 which, following reduction with sodium borohydride, yielded products 5 and 10. The ethyl ester group was removed with sodium hydroxide in water, to furnish the free carboxylic acids 6 and 11, while the primary benzylic alcohol of 7 and 12 was obtained by exhaustive reduction with lithium aluminum hydride from 4 and 9.

To evaluate the role of stereochemistry of the *bis*-trifluoromethyl-1,3-propanediol chain, we attempted separation of the two enantiomers of 5 by means of esterification of the secondary alcohol with a chiral, enantiopure carboxylic acid and then separation of the two diastereomeric products thus obtained [16]. To this end, direct functionalization by esterification of the secondary alcohol with a chiral carboxylic acid (*N*-Boc-L-alanine, as a readily available enantiopure carboxylic acid) of the final product 5 proved unsuccessful. We therefore planned to separate two precursors of the final products, and the successful separation of the enantiomers was accomplished as depicted in Scheme 3.

Condensation/reduction of 4-bromo acetophenone and HFA furnished racemic diol 13. This was condensed with *N*-Boc-L-alanine to furnish diastereomeric 14a and 14b, which could be separated by column chromatography [17]. Following saponification, enantiopure diols 15a and 15b were reacted with 4-carboxyethyl-phenyl boronic acid 18, to give the optical antipodes 16 and 17.

Extending on the biphenyl structural motif, naphthol-derived compounds 22 and 24 were prepared in an analogous manner as depicted in Scheme 4. 6-Bromo-2-naphthol 19 was protected at first as *tert*-butyldimethyl silyl ether (20) [18], followed by Suzuki-Miyaura coupling with 4-acetyl bis(pinacolato)-phenyl boronate or 3-acetyl bis(pinacolato)-phenyl boronate to give isomeric compounds 21 and 23, respectively [19]. These were subjected to the standard condensation/reduction sequence to furnish (after deprotection with TBAF of the silyl ether) compound 22 and compound 24.

The series of open-chain, flexible derivatives comprising two aromatic nuclei required few distinct synthetic operations, depending on

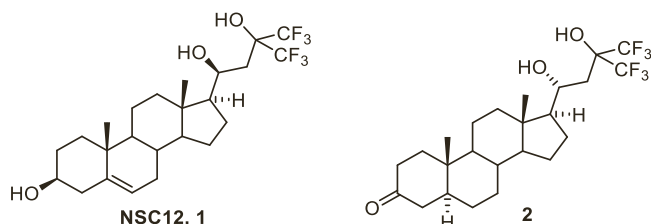
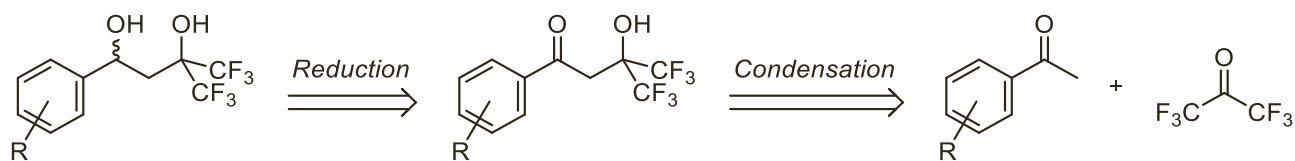
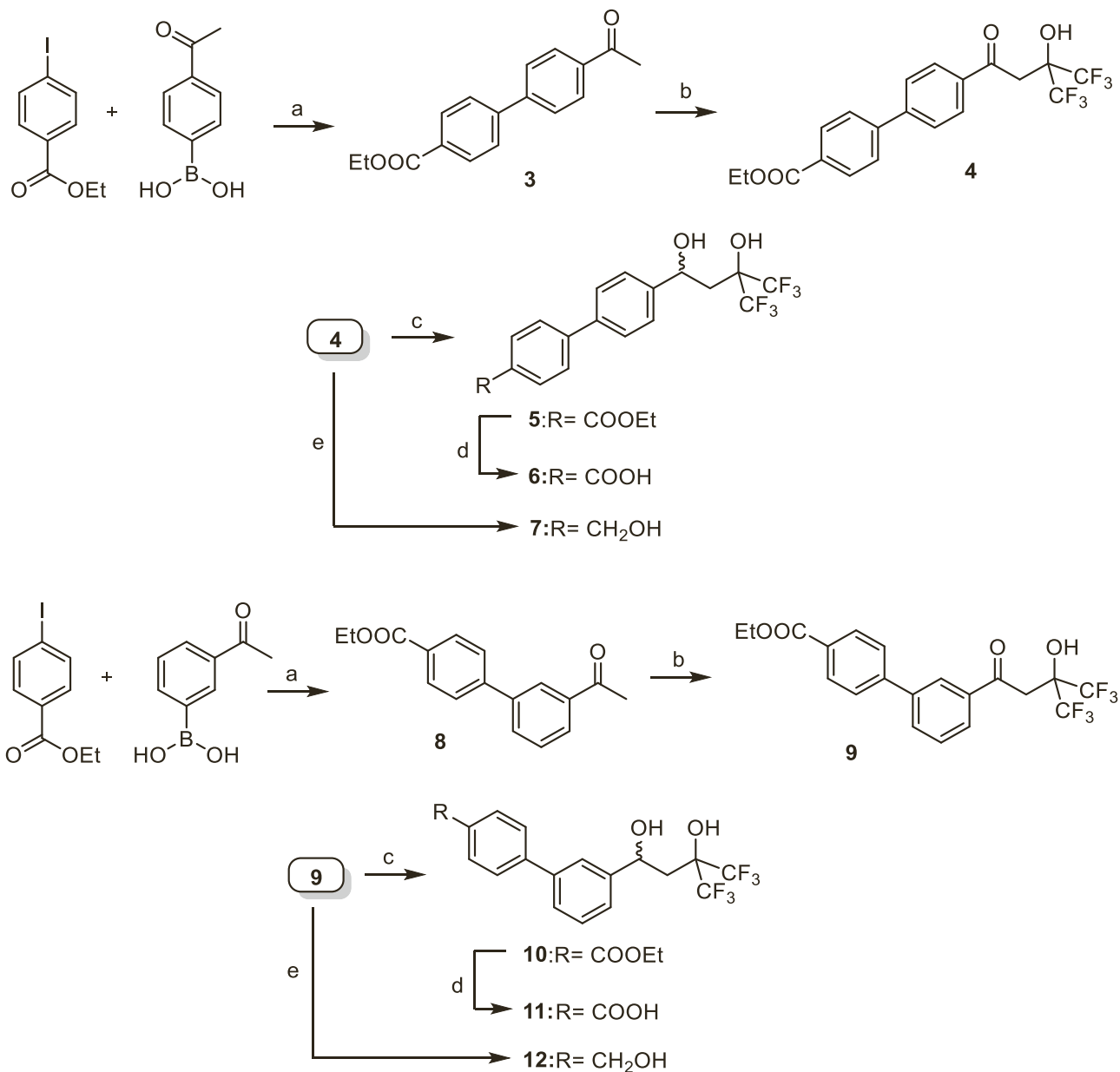


Fig. 1. Chemical structure of FGF trap compounds with steroid scaffold.



Scheme 1. Retrosynthetic strategy.



Scheme 2. Synthesis of compounds 5-7 and 10-12. Reagents and conditions: a) 1,4-dioxane, water, Pd(PPh₃)₂Cl₂, K₂CO₃, 100 °C, 3 h. b) THF, LiHMDS, HFA, -60 °C to rt, 3 h. c) THF, MeOH, NaBH₄, 0 °C, 30 min. d) H₂O, THF, NaOH, rt, 18 h. e) THF, LiAlH₄, 0 °C, 1 h.

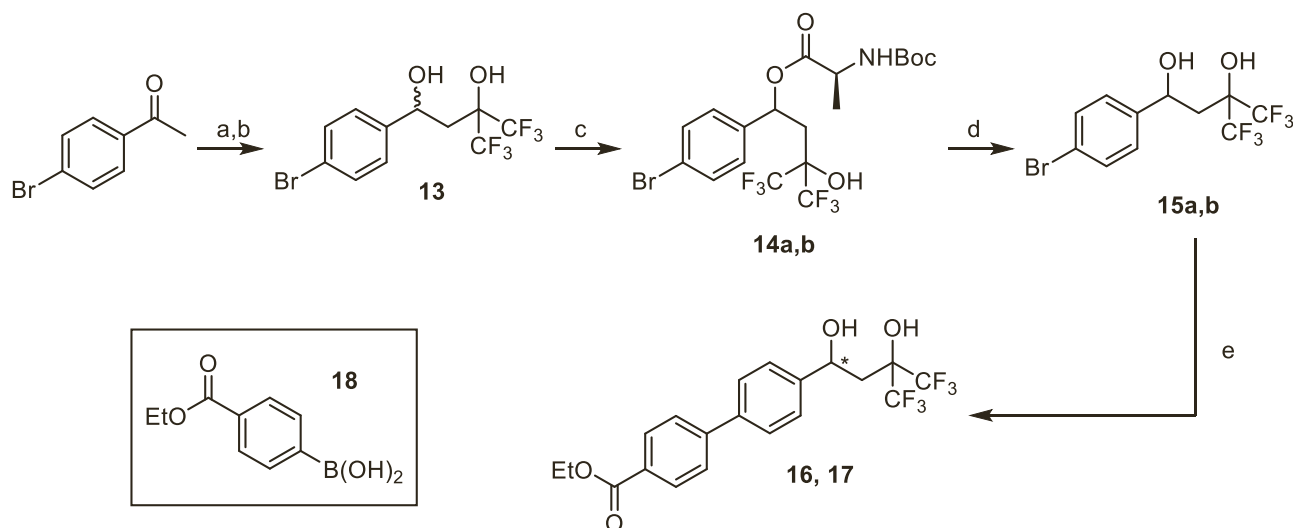
the specific substitution pattern designed.

As depicted in Scheme 5, compounds 26 and 28 were prepared with a unified, straightforward synthesis comprising the alkylation of 4-fluorophenol with either 3-bromomethyl- or 4-bromomethyl acetophenone to give the corresponding *meta*- or *para*-substituted ketones 25 and 27, respectively, that gave, after condensation/reduction with HFA, 26 and 28 [20].

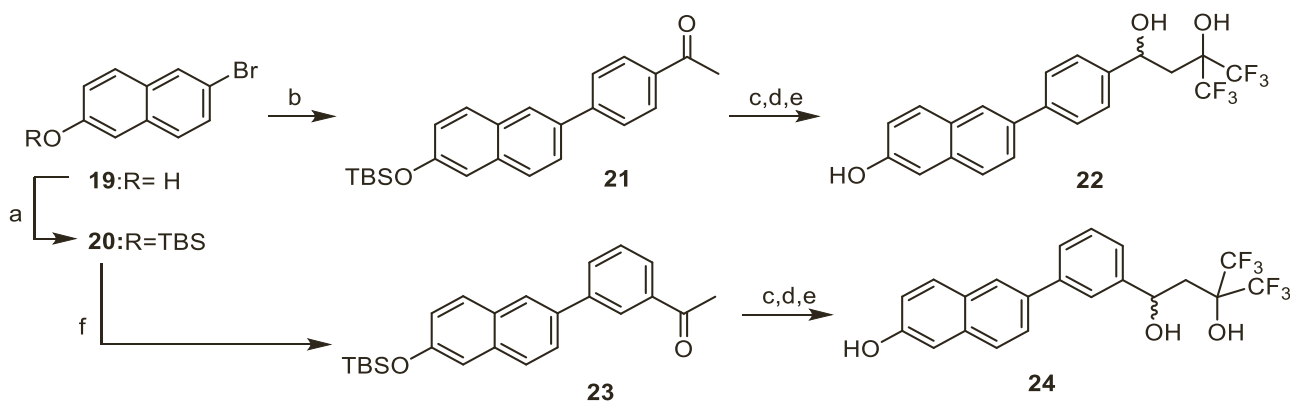
Compounds bearing a methoxy group installed in the *para* position with respect to the propanediol chain were prepared with different

approaches, dictated by the junction between the two aromatic nuclei.

For the preparation of compound 31, we devised a straightforward synthesis that profited of the nucleophilic addition of a lithiated specie directly onto an aldehyde (Scheme 6) [21]. Easily derived adduct 30 (from the alkylation of 4-fluorophenol with 3-chloromethyl-4-methoxy benzaldehyde 29) [22] was treated with a slight excess of the metalated halohydrin derived from the action of *n*-butyllithium on the commercially available 2-(bromomethyl)-1,1,1,3,3,3-hexafluoropropan-2-ol. This reaction gave compound 31 in modest, yet



Scheme 3. Synthesis of enantiomers 16 and 17. Reagents and conditions: a) THF, LiHMDS, HFA, -60°C to rt, 3 h. b) THF, MeOH, NaBH_4 , 0°C , 2 h. c) DCM, *N*-Boc-L-alanine, DMAP, EDCl, 0°C to rt, 18 h. d) MeOH, Na^0 , 0°C to rt 24 h. e) 18, 1,4-dioxane, water, $\text{Pd}(\text{PPh}_3)_2\text{Cl}_2$, K_2CO_3 , reflux, 5 h.



Scheme 4. Synthesis of compounds 22 and 24. Reagents and conditions: a) DMF, TBDMSCl, NEt_3 , 0°C , 24 h. b) 1,4-dioxane, water, 4-acetyl bis(pinacolato)-phenyl boronate, $\text{Pd}(\text{PPh}_3)_2\text{Cl}_2$, K_2CO_3 , reflux, 5 h. c) THF, LiHMDS, HFA, -60°C to rt, 3 h. d) THF, MeOH, NaBH_4 , 0°C , 2 h. e) THF, TBAF, 3 h. f) 1,4-dioxane, water, 3-acetyl bis(pinacolato)-phenyl boronate, $\text{Pd}(\text{PPh}_3)_2\text{Cl}_2$, K_2CO_3 , reflux, 5 h.

useful yield. This protocol, however, proved to be of extremely narrow applicability, due to a very low functional group tolerance. Attempted reaction with the chlorine-functionalized counterpart of 30 (compound 32, Scheme 7) resulted in a complex mixture of products, from which no desired compound could be isolated.

We therefore performed the synthesis of 34, the chlorinated analog of 31, by a different approach depicted in Scheme 7, analogously to 28 and 34 (Scheme 5).

Alkylation of 4-chloro-phenol with 3-chloromethyl-4-methoxy benzaldehyde 29 gave intermediate 32 that was transformed in the corresponding ketone 33 by means of a two-step procedure. At first, methylmagnesium bromide addition to the carbonyl group produced an intermediate secondary alcohol, which was oxidized to the corresponding methyl ketone 33 by a modified Oppenauer oxidation employing an *in situ* generated aluminum-alkoxide (secondary alcohol reacted with 0.33 eq. of trimethylaluminum and cyclohexanone as the terminal oxidant in refluxing toluene [23,24]). Compound 33 could then be condensed with HFA and reduced to the corresponding diol 34.

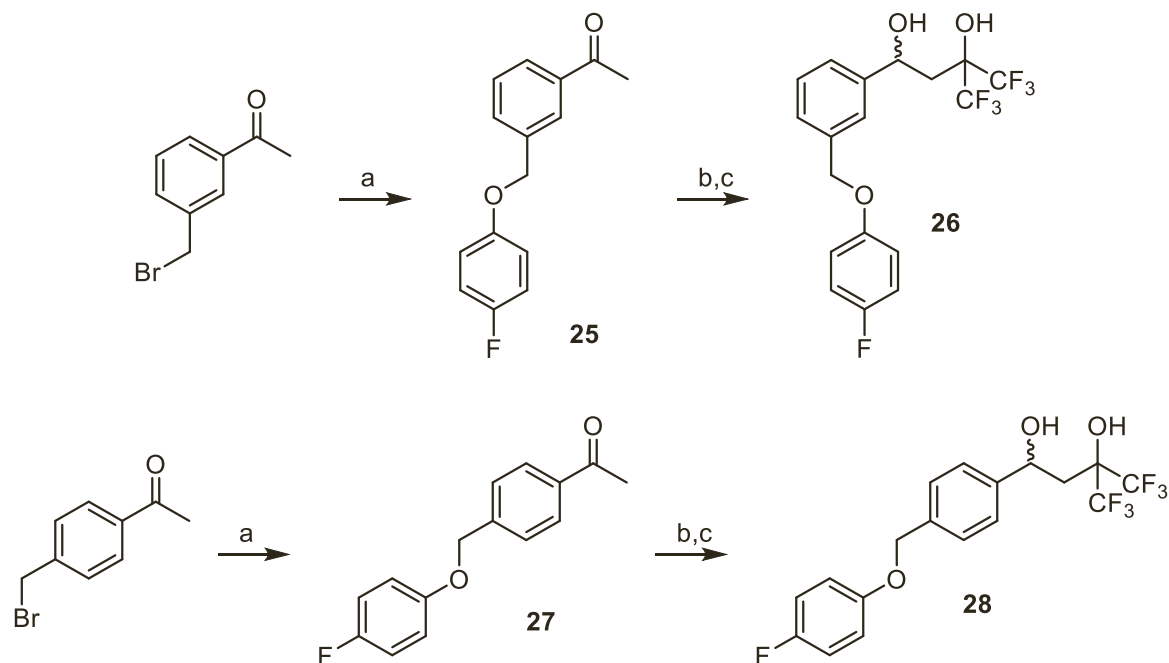
The carbon-chain tethered compound 39 (Scheme 8) required a different synthetic approach. 2-Chloromethyl anisole 35 was transformed in the corresponding Grignard reagent and reacted with 4-fluoro benzaldehyde to give intermediate carbinol 36 [25]. This was reduced employing a two-step reaction sequence comprising at first the conversion of the hydroxyl functionality into the corresponding chloride by

treatment with concentrated hydrochloric acid, followed by reduction with zinc, to furnish compound 37 [26,27]. Regioselective Friedel-Crafts acylation gave methyl-ketone 38, and standard condensation/reduction finally gave 39 [28,29].

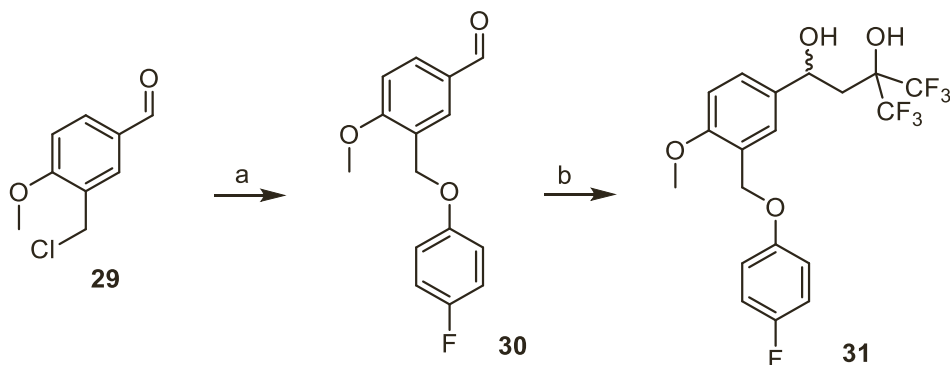
Compounds bearing an amide group to act as the hinge motif were prepared starting from 3-nitro-4-methoxy acetophenone 40 (Scheme 9) [30]. This was directly condensed with HFA to furnish compound 41, that was subjected to two distinct reduction steps to obtain intermediate 42, condensed with 4-fluorobenzoyl chloride to furnish 43. *N*-methyl functionalized compound 47 could by no mean be obtained by either 42 or 43 and was prepared separately from 3-amino-4-methoxy acetophenone 44, that was condensed with 4-fluorobenzoyl chloride to give 45, alkylated with iodomethane to give 46, which was condensed with HFA and reduced to diol 47.

Conformationally constrained compounds 50 and 51 were prepared as depicted in Scheme 10. Alkylation of 4-fluorophenol with ketone 48 [31] furnished compound 49 that was subjected to condensation with HFA to give 50 and, following reduction, 51, obtained as a racemic mixture of *trans*-configured isomers.

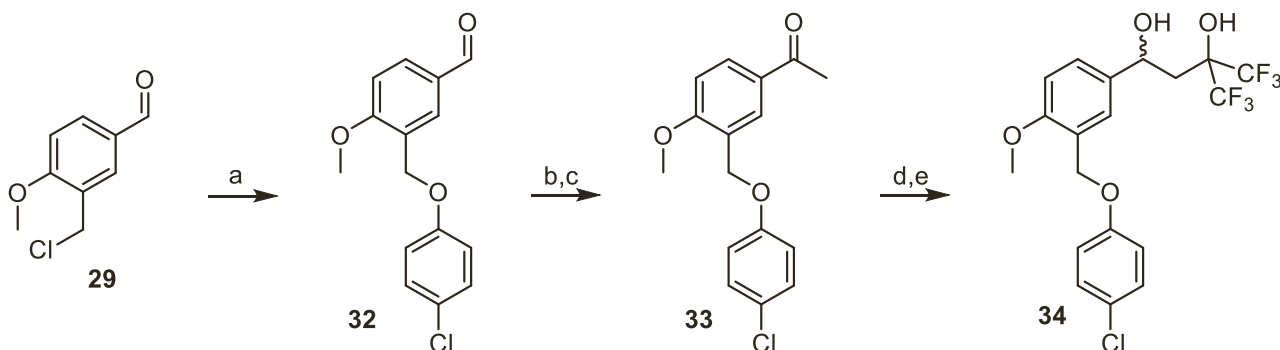
The merging of the pharmacophores of 22 and 26 was accomplished by synthesizing 57, as depicted in Scheme 11. Compound 20 was converted into boronate ester 52 [32], which was subjected to Suzuki-Miyaura cross coupling reaction with methyl-ketone 53. Following reaction of 54 with 4-fluoro phenol, compound 56 was



Scheme 5. Synthesis of compounds **26** and **28**. Reagents and conditions: a) DMF, 4-fluorophenol, K_2CO_3 , rt 15 h. b) THF, LiHMDS, HFA, $-60^\circ C$ to rt. c) THF, MeOH, $NaBH_4$, $0^\circ C$, 30 min.



Scheme 6. Synthesis of compound **31**. Reagents and conditions: a) DMF, 4-fluorophenol, K_2CO_3 , rt, 18 h. b) i) 2-(bromomethyl)-1,1,1,3,3,3-hexafluoropropan-2-ol, THF, $n-BuLi$, $-78^\circ C$; ii) **30**, $-78^\circ C$ to $-30^\circ C$.

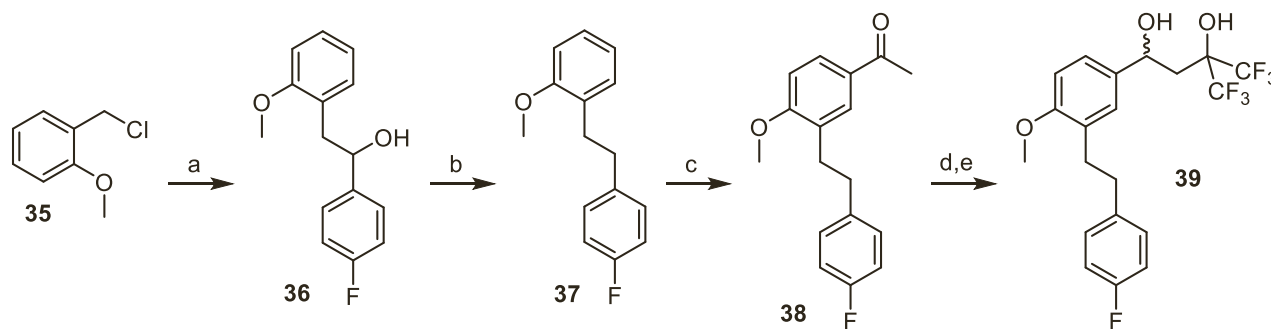


Scheme 7. Synthesis of compound **34**. Reagents and conditions: a) DMF, 4-chlorophenol, K_2CO_3 , rt, 18 h. b) THF, $MeMgBr$, $0^\circ C$, 20 min. c) i) Toluene, $Al(CH_3)_3$, $0^\circ C$, 20 min; ii) Toluene, cyclohexanone, reflux, 2 h. d) THF, LiHMDS, HFA, $-60^\circ C$ to rt, 4 h. e) THF, MeOH, $NaBH_4$, $0^\circ C$, 1 h.

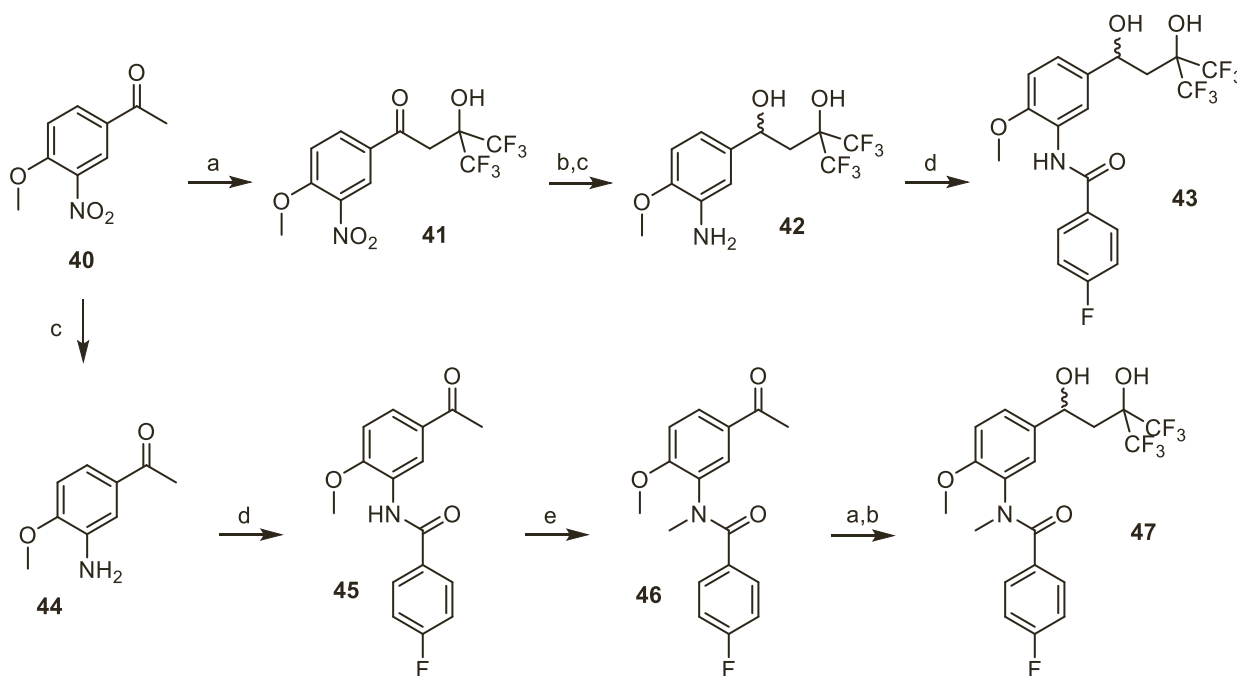
obtained by condensation of **55** with HFA, followed by removal of the silyl ether protecting group. Reduction with sodium borohydride in methanol furnished compounds **57**.

Finally, control compound **59** was prepared employing 2-nonanone

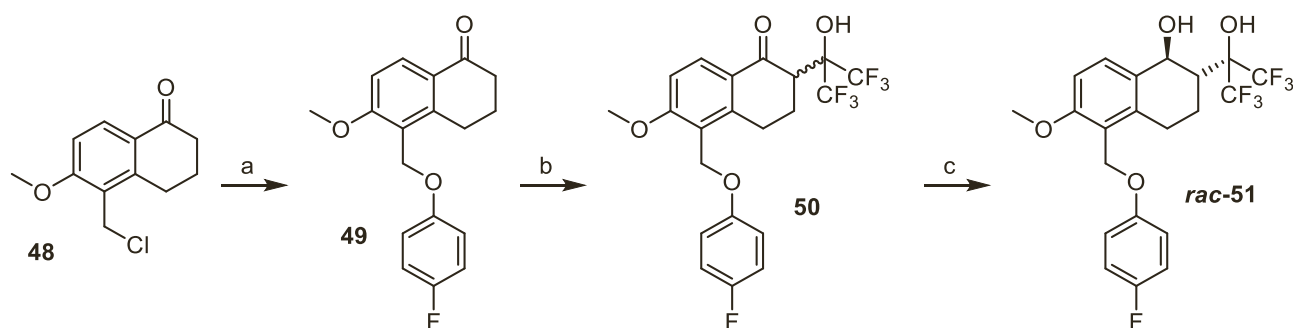
58 as the starting material, which reacted with HFA and the intermediate β -hydroxy-ketone was reduced with sodium borohydride (Scheme 12).



Scheme 8. Synthesis of compound 39. Reagents and conditions: a) i) THF, Mg⁰, reflux, 30 min; ii) THF, 4-fluorobenzaldehyde, 0 °C, 30 min. b) i) HCl 37 %, 30 min, rt; ii) Et₂O, AcOH, Zn⁰, reflux, 60 min. c) DCM, AlCl₃, Ac₂O, 0 °C, 20 min. d) THF, LiHMDS, HFA, -60 °C to rt, 4 h. e) THF, MeOH, NaBH₄, 0 °C, 30 min.



Scheme 9. Synthesis of compounds 43 and 47. Reagents and conditions: a) THF, LiHMDS, HFA, -60 °C to rt, 1 h. b) MeOH, NaBH₄, 0 °C, 30 min. c) EtOH, water, AcOH, Fe⁰, rt, 3 h. d) 4-fluorobenzoyl chloride, pyridine, 30 min, rt. e) THF, NaH, MeI, 0 °C, 2.5 h.



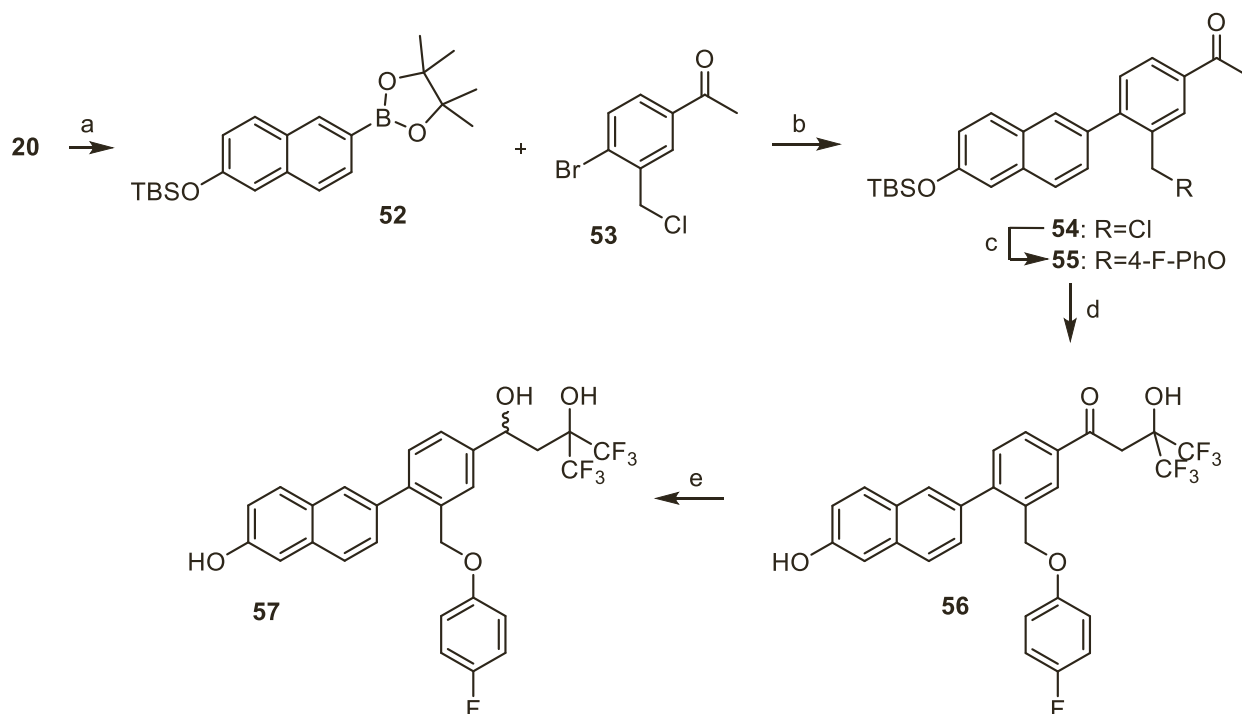
Scheme 10. Synthesis of compounds 50 and 51. Reagents and conditions: a) DMF, 4-fluorophenol, K₂CO₃, rt, 18 h. b) THF, LiHMDS, HFA, -60 °C to rt, 3 h. c) MeOH, NaBH₄, 0 °C, 30 min.

3. Results

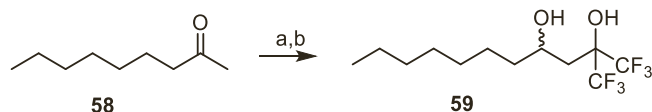
3.1. Structure-activity relationships

Non-steroidal NSC12 derivatives were evaluated by Western blot analysis (Fig. 2 and Figure S1) for their ability to hamper the autocrine

activity exerted by FGFs secreted by MM KMS-11 cells in which a t(4;14) chromosomal translocation leads to FGFR3 overexpression and FGF-dependent signaling hyperactivation [33]. Inhibition of FGFR3 phosphorylation was used as an index of this inhibitory activity when KMS-11 cells were incubated with the compound under test at the fixed concentration of 6 μM (Table 1). This concentration was considered



Scheme 11. Synthesis of compound 56. Reagents and conditions: a) 1,4-dioxane, B_2Pin_2 , Pd(Dppf)Cl₂, AcOK, 90 °C, 6 h. b) 1,4-dioxane, water, Pd(PPh₃)₂Cl₂, K₂CO₃, reflux, 7 h. c) DMF, 4-fluorophenol, K₂CO₃, rt 18 h. d) (i) THF, LiHMDS, HFA, -60 °C to rt, 3 h. (ii) THF, TBAF, 3 h. e) THF, MeOH, NaBH₄, 0 °C, 1 h.



Scheme 12. Synthesis of compound 59. Reagents and conditions: a) THF, LiHMDS, HFA, -60 °C to rt, 3 h. b) MeOH, NaBH₄, 0 °C, 30 min.

suitable for compound screening based on dose-response curves previously obtained for NSC12 (1) showing about 80 % inhibition of FGFR3 activation at 6 μ M [13].

A biphenyl scaffold carrying a hydroxymethyl substituent in para position was initially evaluated as a possible alternative to the steroid portion of NSC12. Unfortunately, insertion of the 1,1-bis-trifluoromethyl-1,3-propanediol side chain in either para (7) or meta (12) position did not provide active compounds. Replacement of the

hydroxymethyl with a hydrophilic carboxylic group led to the inactive compound 6 and to compound 11 that showed a limited ability to inhibit FGFR3 phosphorylation (41 %). Introduction of a lipophilic ethoxycarbonyl group was more successful, with the para-substituted derivative 5 and the meta-substituted 10 showing 51 % and 31 % inhibition of FGFR3 phosphorylation, respectively. The enantiomers of the most potent compound 5, 16 and 17, were tested separately, showing no improvement over the racemic mixture, nor relevance of stereochemistry on compound efficacy.

Based on the results obtained for biphenyl derivatives, we speculated that an increase of lipophilicity would be favorable for interaction with FGF. Thus, we extended the aromatic scaffold by preparing β -(phenyl)naphthyl derivatives. These compounds carry a hydroxyl group in position 6 of the naphthyl ring mimicking that of NSC12 (1) and were substituted with the 1,1-bis-trifluoromethyl-1,3-propanediol chain in para (22) or meta (24) position of the phenyl ring. Modification of the

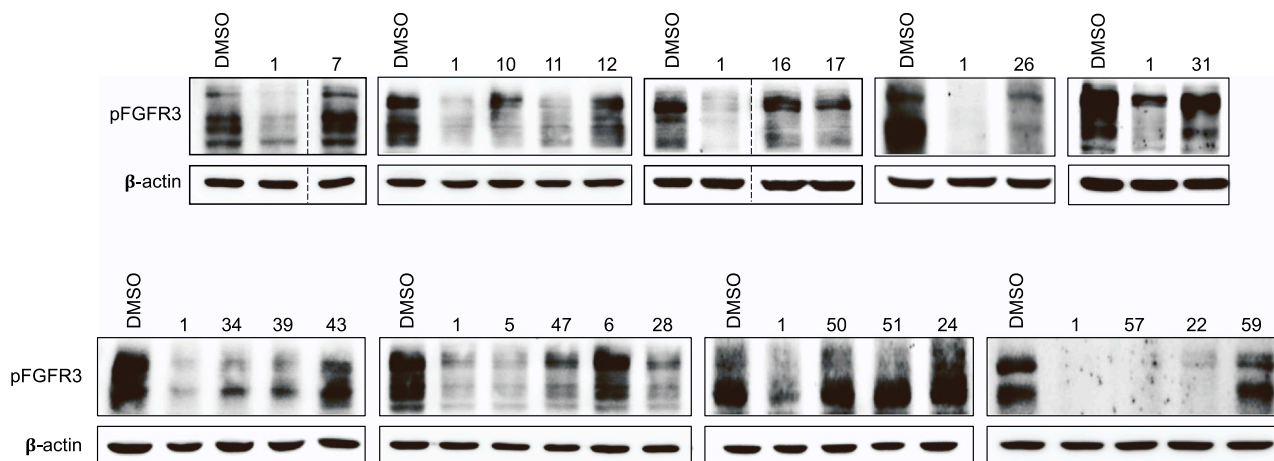
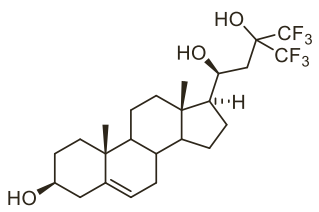
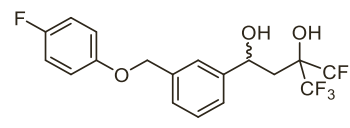
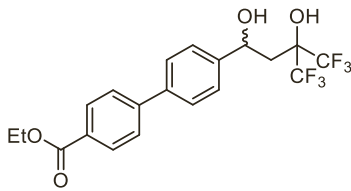
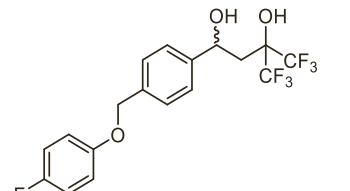
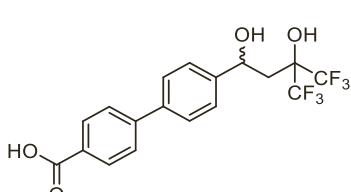
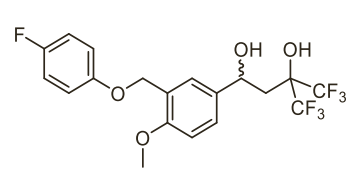
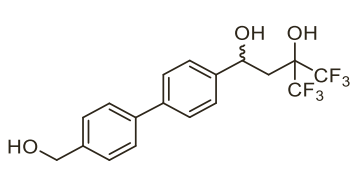
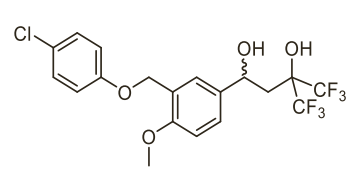
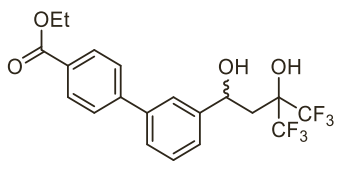
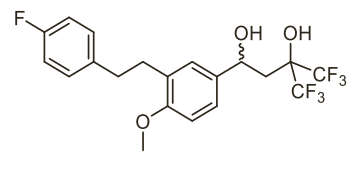
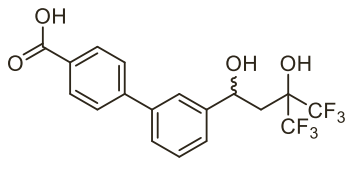
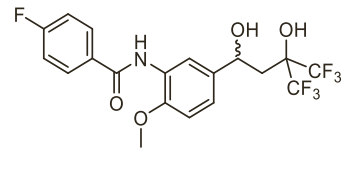
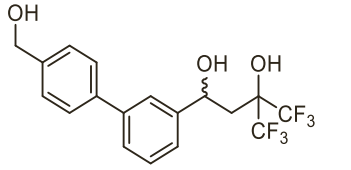
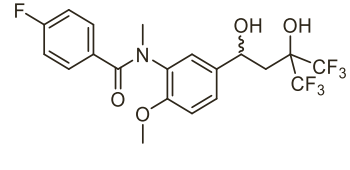


Fig. 2. Western blot analysis of FGFR3 phosphorylation (pFGFR3) after treatment of KMS-11 cells with NSC12 (1) or non-steroidal derivatives for 6 hours at 6 μ M concentration. β -Actin was used as loading control.

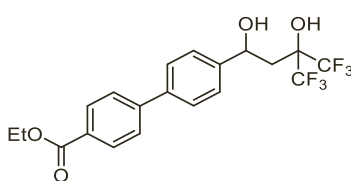
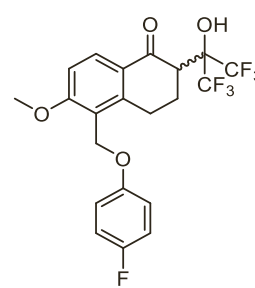
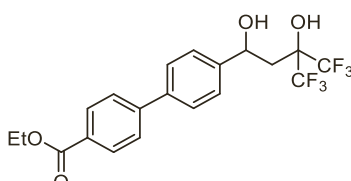
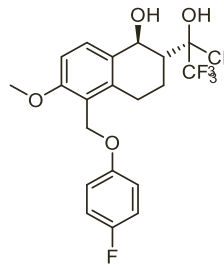
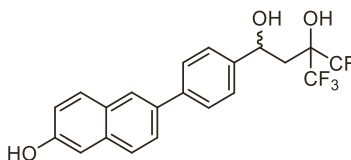
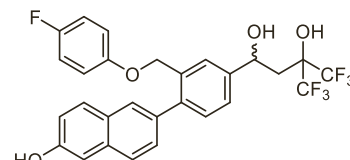
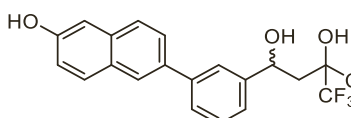
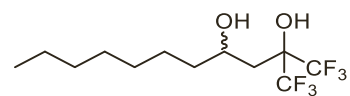
Table 1

Percentage of inhibition of FGFR3 phosphorylation in KMS-11 cells after treatment of KMS-11 cells with NSC12 (1) or non-steroidal derivatives for 6 hours at 6 μ M concentration.

Compd. ^a	pFGFR3%inhib.	Compd. ^a	pFGFR3% inhib.
NSC12 (1)	75	26	65
			
5	51	28	40
			
6	inactive ^c	31	20
			
7	inactive ^c	34	45
			
10	31	39	39
			
11	41	43	16
			
12	10	47	25
			

(continued on next page)

Table 1 (continued)

Compd. ^a	pFGFR3%inhib.	Compd. ^a	pFGFR3% inhib.
(-)-16 ^b	22	50	inactive ^c
			
(+)-17 ^b	35	51	inactive ^c
			
22	75	57	74
			
24	inactive ^c	59	inactive ^c
			

^a Compounds were tested as racemic mixtures.

^b Single enantiomer.

^c Inactive: < 10 %.

lipophilic portion gave the desired result, as the para derivative **22** showed the same % of inhibition of FGFR3 phosphorylation as NSC12 (**1**). The different spatial arrangement of substituents in compound **24** was not favorable and led to an inactive compound.

Next, we looked for more flexible open-ring derivatives, in which the benzene carrying the 1,1-bis-trifluoromethyl-1,3-propanediol chain was connected through a methyleneoxy linker to another phenyl ring which replaces the naphthyl core of compounds **22** and **24**. The fluorine atom on the terminal phenyl ring could interact with target FGFs while being less prone to metabolic transformation than the hydroxyl group of NSC12 (**1**). Both the para- (**28**) and meta-substituted (**26**) compounds gave an appreciable inhibition of FGFR phosphorylation (40 and 65 %, respectively). We therefore set up a SAR exploration of the more potent compound **26**. A methoxy group was inserted ortho to the methyleneoxy linker to increase lipophilicity (**31**), a chlorine replaced the fluorine atom (**34**), and different linkers were evaluated, i.e., a dimethylene chain in compound **39**, or an amide and N-methylamide in analogs **43** and **47**, respectively. These derivatives did not reach the inhibitory potency of the parent **26**, with worse results recorded for the more hydrophilic amide derivatives.

Compounds **50** and **51** are conformationally constrained derivatives of the potent inhibitor **26** in which the 1,1-bis-trifluoromethyl-1,3-propanediol side chain was partially included in a tetralin ring. These compounds were designed to provide information on the spatial relationship between the side chain and the aromatic portion of the flexible non-steroidal FGF traps. Unfortunately, the reduction in conformational

flexibility did not allow to maintain an effective inhibition of FGFR3 phosphorylation and both derivatives were inactive.

Finally, given the highest potencies observed for the β -(phenyl)-naphthyl compound **22** and the open-ring derivative **26**, we combined the two structures in compound **57** in which the central phenyl ring carries both the naphth-6-ol portion and the p-F-phenoxy chain. The compound showed the same activity as the parent **22** and proved that the two pharmacophore portions are mutually tolerated, even though they do not exhibit an additive effect. The simplified structure of non-steroidal FGF trap inhibitors, in which different aromatic scaffolds can be coupled with the 1,1-bis-trifluoromethyl-1,3-propanediol side chain, poses the question if the lipophilic portion has a specific role in the interaction with FGF or merely confers a suitable lipophilic character. We prepared compound **59**, in which the 1,1-bis-trifluoromethyl-1,3-propanediol chain was conjugated with a simplified linear lipophilic alkyl tail. The lack of inhibitory activity of this compound confirms the importance of structural complementarity with target FGF to affect FGFR phosphorylation.

On these bases, compounds **22** and **57**, together with compound **59** as a negative control, were further investigated for their FGF trap feature and anti-myeloma activity.

3.2. Compounds **22** and **57** act as FGF traps

The FGF trap activity of compounds **22** and **57** was evaluated by assessing their capacity to interact with FGF2 that represents the

prototype member of the FGF family [34]. First, *in silico* and surface plasmon resonance (SPR) analyses were performed. Previous molecular modeling studies had shown that NSC12 (1) may interact with a region of the FGF2 molecule involved in FGFR binding, thus explaining its FGF inhibitory activity [11]. Accordingly, blind docking based on AutoDock Vina [35] identifying putative binding sites on the surface of FGF2 (PDB ID 1FQ9) highlighted a binding cluster for the screened compounds similar, but not identical, to NSC12 (1). This cluster was related to an “internal” portion of FGF2 involved in the interaction with FGFR1, as can be deduced by the analysis of crystallographic structures (e.g., 1FQ9, 1CVS, 1EV2, 5W59, 4J23, 1EVT) (Fig. 3A). It can be noted that the trifluoromethyl groups of all ligands are superimposed, thus sustaining the relevant role for this portion of the molecules in the interaction with the target [13]. This docking analysis identified also a second binding cluster placed in an “external” site of the FGF2 molecule which is not involved in the interaction of the growth factor with neither its receptors nor HSPGs (Figure S2).

Further, molecular dynamics simulations were carried out using PlayMolecule [36] starting from the best scoring docking pose of each compound on both sites (3 replicates of 25 ns). These simulations showed a higher dynamic stability for the “internal” poses (Fig. 3B). Thus, “external” poses were not analyzed further.

Finally, the behavior of the compounds under test in the “internal” pose was investigated more in depth by means of binding pose

metadynamics (BPMD) of the Schrödinger suite [37]. This protocol, which relies on the well-tempered metadynamics approach, allows to assess the stability of a small molecule in its binding pose by adding a time-dependent bias as function of a collective variable (CV) able to sample the movements of the ligand around its binding pose. The CV was defined as the root mean square deviation (RMSD) from the equilibrated starting pose. BPMD provides a result termed PoseScore, which is indicative of the average RMSD from the equilibrated starting pose. The BPMD protocol should favor the displacement from the equilibrated pose of ligands with a low binding affinity, thus scoring a high PoseScore, while more potent compounds, characterized by a higher binding affinity and by more stable protein-ligand interactions, would feature a lower PoseScore. Analysis of the PoseScore values obtained from BPMD simulations on FGF traps showed that the interaction of compound 57 with FGF2 was the most stable, followed by compound 22, and NSC12 (1). The inactive compound 59 showed the less stable interaction (Fig. 3C).

The FGF trap affinity of compounds 22 and 57 was further confirmed experimentally by assessing their capacity to bind FGF2 immobilized to a BIAcore sensor chip (Fig. 3D), as already shown for the reference compound NSC12 (1) [11]. Indeed, the SPR binding isotherms revealed a dissociation constant (K_d) of about 51 μM for compound 22, similar to that measured for NSC12 (1) [11], while a higher FGF2 binding affinity was observed for the branched compound 57 ($K_d \sim 24 \mu\text{M}$), suggesting

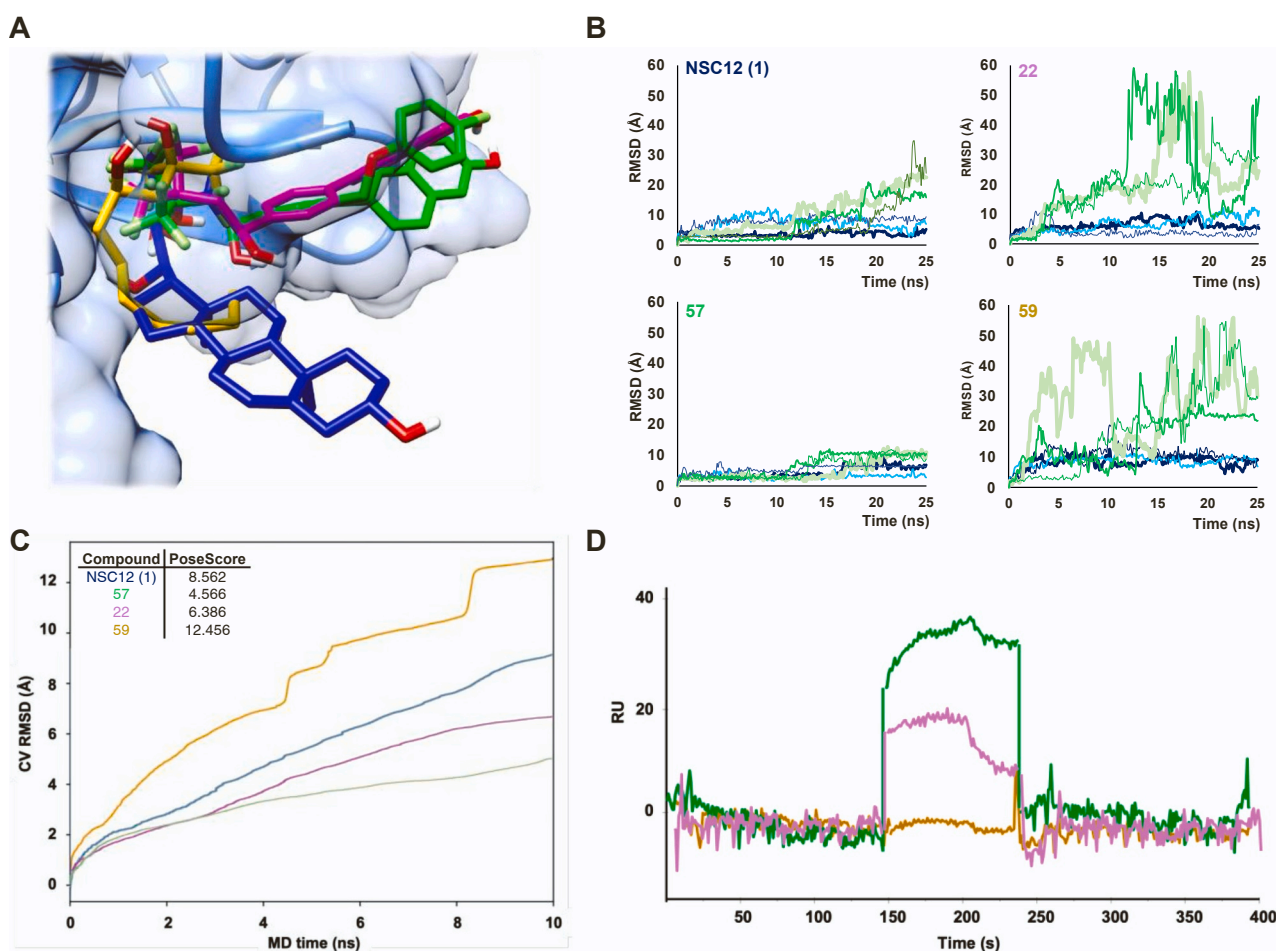


Fig. 3. Computational and experimental studies investigating the interaction of NSC12 (1), compounds 22, 57 and 59 with FGF2. (A) Molecular docking studies. The best scoring poses in the “internal” site are shown for all the compounds, color code: NSC12 (1) (in blue), 57 (in green), 22 (in magenta), 59 (in yellow); detailed views of docking poses are depicted in Fig. S3. (B) MD simulations carried out for the compounds docked on the “internal” and “external” FGF2 sites. RMSD are reported in green (external pose) and in blue (internal pose). Simulations were performed in triplicate. (C) BPMD simulations starting from the internal poses; PoseScore values are reported in the inset of the figure. (D) Binding isotherms from SPR analyses for the interaction with FGF2; color code: 57 (in green), 22 (in magenta), 59 (in yellow).

that the two pharmacophore portions both concur to binding interactions. The inactive compound **59** was unable to efficiently bind FGF2 (Kd > 150 μ M), confirming the specificity of the interaction of compounds **22** and **57**.

To further confirm these findings, NSC12 derivatives **22** and **57** were assessed for their capacity to prevent the formation of HSPG/FGF/FGFR ternary complexes, essential for FGF-mediated receptor activation and signal transduction [2]. To this aim, a cell-cell adhesion assay was used based on the capacity of FGF2 to interact simultaneously in *trans* with HSPGs and FGFR1 expressed on neighboring HSPG- and FGFR1-overexpressing CHO cells, thus causing FGF-mediated cell-cell adhesion [38]. As shown in Fig. 4A, compounds **22** and **57** significantly inhibited the formation of HSPG/FGF2/FGFR1 ternary complexes with a potency higher than NSC12 (**1**), whereas compound **59** was devoid of significant activity. Accordingly, compounds **22** and **57** were able to hamper FGFR activation in FGFR1-overexpressing CHO cells stimulated with FGF2. Indeed, Western blot analysis performed using a pan-phosphoFGFR (pFGFR) antibody demonstrated that both compounds significantly inhibited FGFR1 phosphorylation (Fig. 4B). Again, in keeping with its inability to hamper the formation of HSPG/FGF2/FGFR1 ternary complexes, compound **59** was not able to prevent FGFR activation.

Altogether, the results demonstrate that, like NSC12 (**1**), non-steroidal derivatives **22** and **57** exert their FGF trap activity by binding the FGF domain involved in the interaction with FGFR, thus preventing the formation of HSPG/FGF/FGFR ternary complexes, FGFR phosphorylation, and activity.

3.3. Compounds **22** and **57** block the growth and survival of MM cell lines

We have previously demonstrated that NSC12 (**1**) inhibits the growth and survival of several cancer cell lines, including MM cells [11,39–41]. In order to test the antitumor activity of compounds **22** and **57**, inhibition of FGFR activation and viable cell counting was assessed on three different MM cell lines, harboring (KMS-11 and OPM-2) or not (U-266) the t(4;14) translocation [41]. Like NSC12 (**1**), both compounds **22** and **57** strongly reduced the levels of FGFR phosphorylation in all cell lines tested, as revealed in Western blot analysis using a pan-pFGFR antibody (Fig. 5A). The inhibition of FGFR activation was paralleled by a significant reduction of cell proliferation (Fig. 5B) and survival (Figure S4).

Previous observations had shown that NSC12 (**1**) exerts a potent oncosuppressive effect also on MM cells resistant to bortezomib, an FDA-approved drug for MM treatment [41]. Importantly, compounds **22** and **57** exerted an inhibitory effect on bortezomib-resistant KMS-11 cells

(KMS-11/BTZ) similar to that observed for bortezomib sensitive MM cell lines tested (Fig. 5 and Figure S4), suggesting that non-steroidal NSC12 derivatives may exert their antitumor activity also in MM cells from those patients relapsed/refractory to proteasome inhibitors. Again, in keeping with all previous experiments, the control compound **59** was devoid of any antitumor activity.

In a previous work [41] we characterized the molecular mechanism by which NSC12 exerts antitumor activity in MM. Indeed, we showed that FGF/FGFR inhibition induces the rapid proteasomal degradation of the oncoprotein c-Myc that is paralleled by mitochondrial oxidative stress, DNA damage and eventually apoptotic tumor cell death. As shown in Fig. 6, the same antitumor molecular mechanism is shared by compounds **22** and **57**. Indeed, treatment with NSC12, compound **22** or **57** strongly reduced the protein levels of c-Myc (Fig. 6A) and induced mitochondrial ROS production (Fig. 6B). These effects were paralleled by DNA damage and apoptotic cell death as shown by significant increased levels of the DNA marker γ H2AX and the cleavage of caspase 3, respectively (Fig. 6A). Again, these effects were not observed after treatment with the control compound **59** (Fig. 6).

3.4. Compounds **22** and **57** strongly reduce the growth of MM tumor xenografts *in vivo*

Based on *in vitro* results, we further assessed the anti-myeloma activity of compounds **22** and **57** *in vivo*. To this aim, NOD/SCID mice were injected subcutaneously with KMS-11 cells and when tumors were palpable, mice were randomly assigned to receive intraperitoneal treatment with NSC12 (7.5 mg/kg), compound **22** (7.5 mg/kg), compound **57** (7.5 mg/kg) or control/vehicle DMSO. As shown in Fig. 7A, the tumor growth resulted significantly slowed down in mice treated with NSC12 derivatives **22** or **57** compared to the growth of tumors in control mice (vehicle). Accordingly, a strong reduction of the weight of treated tumors was observed after harvesting (Figure 7B, C). Interestingly, compound **57** significantly exerted a stronger antitumor activity compared to NSC12 and compound **22**. Indeed, treatment with compound **57** reduced tumor growth of about 60 %, whereas tumor growth was reduced of about 40 % after treatment with NSC12 or compound **22** (Fig. 7A).

Next, immunohistochemical analyses were performed on tumor specimens to confirm *in vivo* the mechanism of action of compounds **22** and **57**. In keeping with previous observations about the antitumor mechanism of NSC12 [41] and here confirmed *in vitro* in KMS-11 cells (see Fig. 6), treatments with NSC12, compound **22** or **57** strongly reduced tumor FGFR phosphorylation also *in vivo* (Fig. 7D). As observed

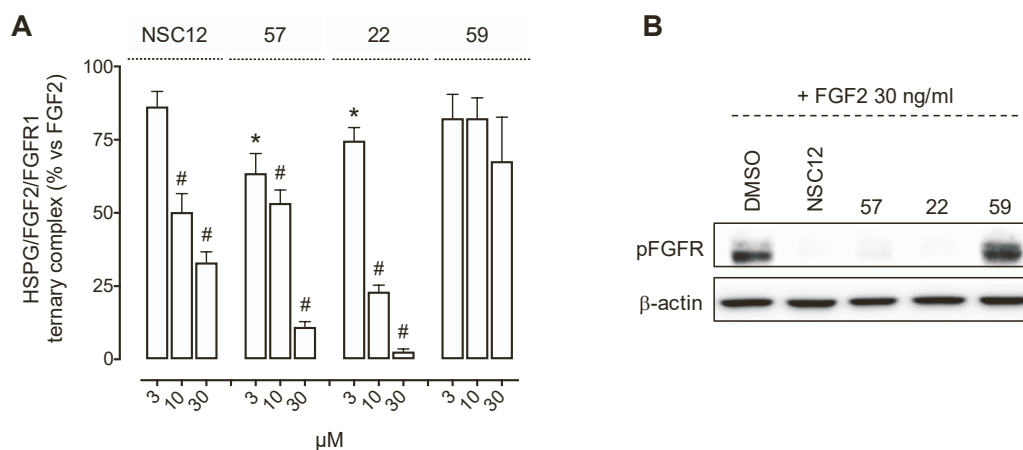


Fig. 4. NSC12 non-steroidal derivatives **22** and **57** disrupt the formation of the bioactive HSPG/FGF2/FGFR1 ternary complex. (A) FGF2-mediated cell-cell adhesion assay by using increasing doses of the testing compounds. Data are mean \pm SEM (n = at least 6 replicates) and expressed as percentage over the controls exposed to FGF2 in absence of the testing compounds. (B) Western blot analysis of the levels of FGFR phosphorylation in FGFR1-overexpressing CHO cells stimulated for 30 minutes with FGF2 in the absence or presence of NSC12 (**1**) or compounds **22**, **57**, and **59**. β -Actin was used as protein loading control. * p<0.05; # p<0.001.

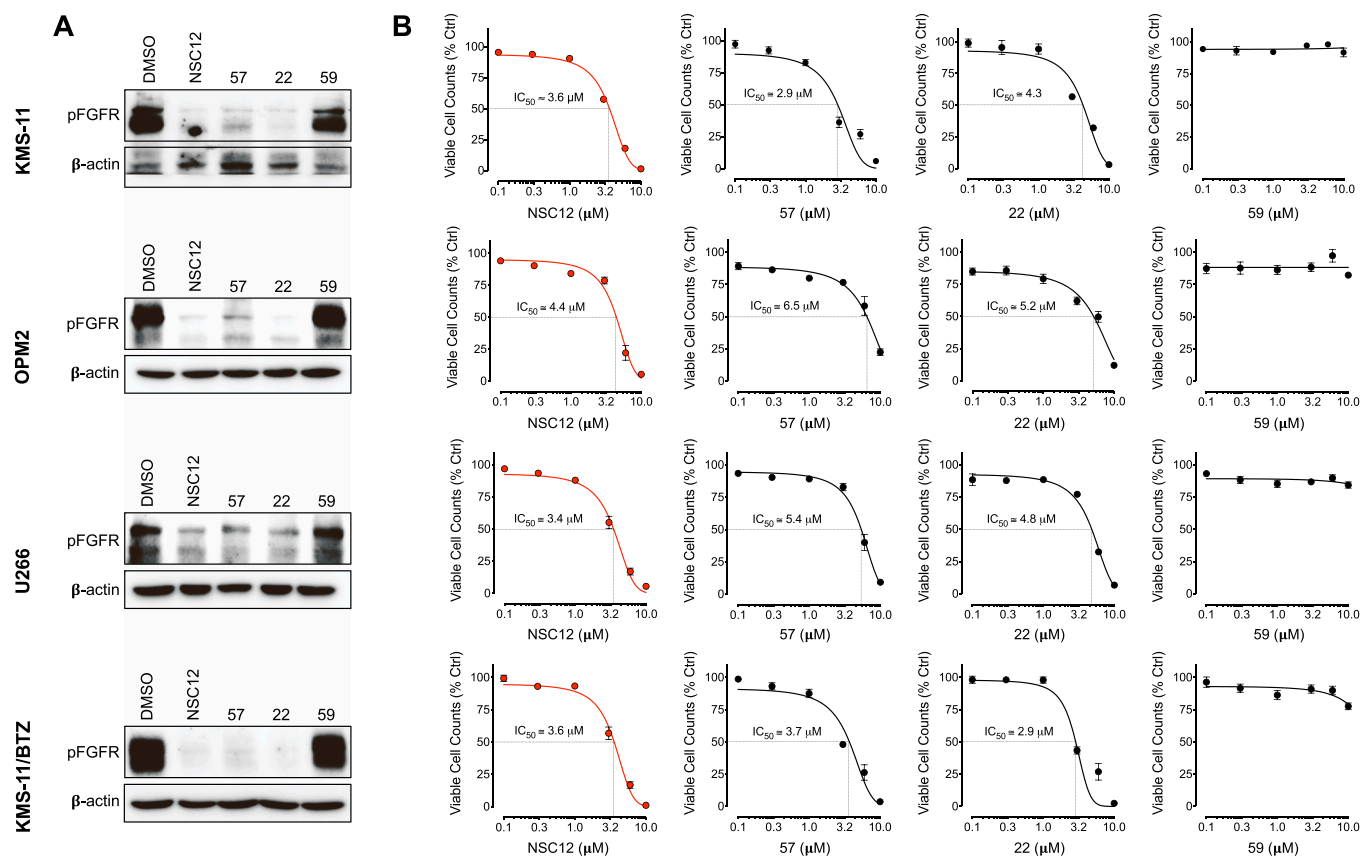


Fig. 5. NSC12 derivatives exert an oncosuppressive effect on different MM cell lines. (A) Western blot analysis of the indicated MM cell lines after 6-hour treatment with NSC12 (1) or non-steroidal derivatives 22, 57 and 59 at 6 μM concentration. (B) Viable cell counting after 48-hour treatment with increasing doses of NSC12 (1) or non-steroidal derivatives 22, 57 and 59. Data are mean ± SEM (n = at least 3 replicates).

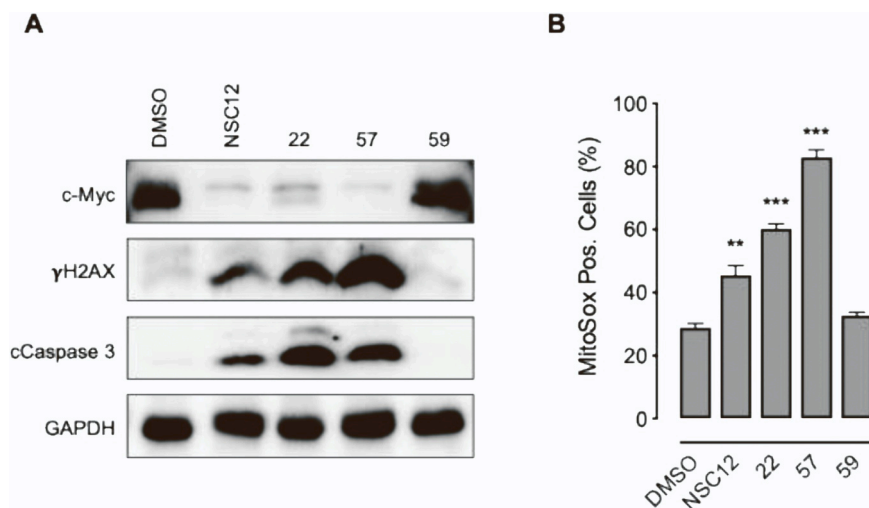


Fig. 6. NSC12 derivatives induce c-Myc degradation, mitochondrial oxidative stress, DNA damage and apoptotic cell death. KM-11 cells were treated for 6 hours with NSC12, compound 22, compound 57 or compound 59 at 6 μM concentration. (A) Western blot analysis. GAPDH was used as loading control. (B) Mitochondrial ROS detection by MitoSox staining and cytofluorimetric analysis of positive cells (n = at least 3 replicates).

in vitro, *in vivo* FGF trapping significantly reduced the levels of c-Myc and this was paralleled by a strong increase of tissue oxidative stress and DNA damage as revealed by nitrotyrosine and γH2AX staining, respectively (Fig. 7D). These effects caused a significant reduction of tumor cell proliferation and survival as assessed by the proliferative marker pHH3 and the apoptotic marker cleaved caspase 3, respectively (Fig. 7D).

Importantly, the anti-myeloma activity of both NSC12 derivatives occurred in the absence of any sign of toxicity. Indeed, no significant changes in the body weight of treated animals was observed (Figure S5A). Also, treatments with compounds 22 and 57 did not significantly affect blood cell composition and biochemical parameters (Figure S5B). Interestingly, in contrast to the hyperphosphatemic effect observed after treatment with FGFR TK inhibitors both in preclinical

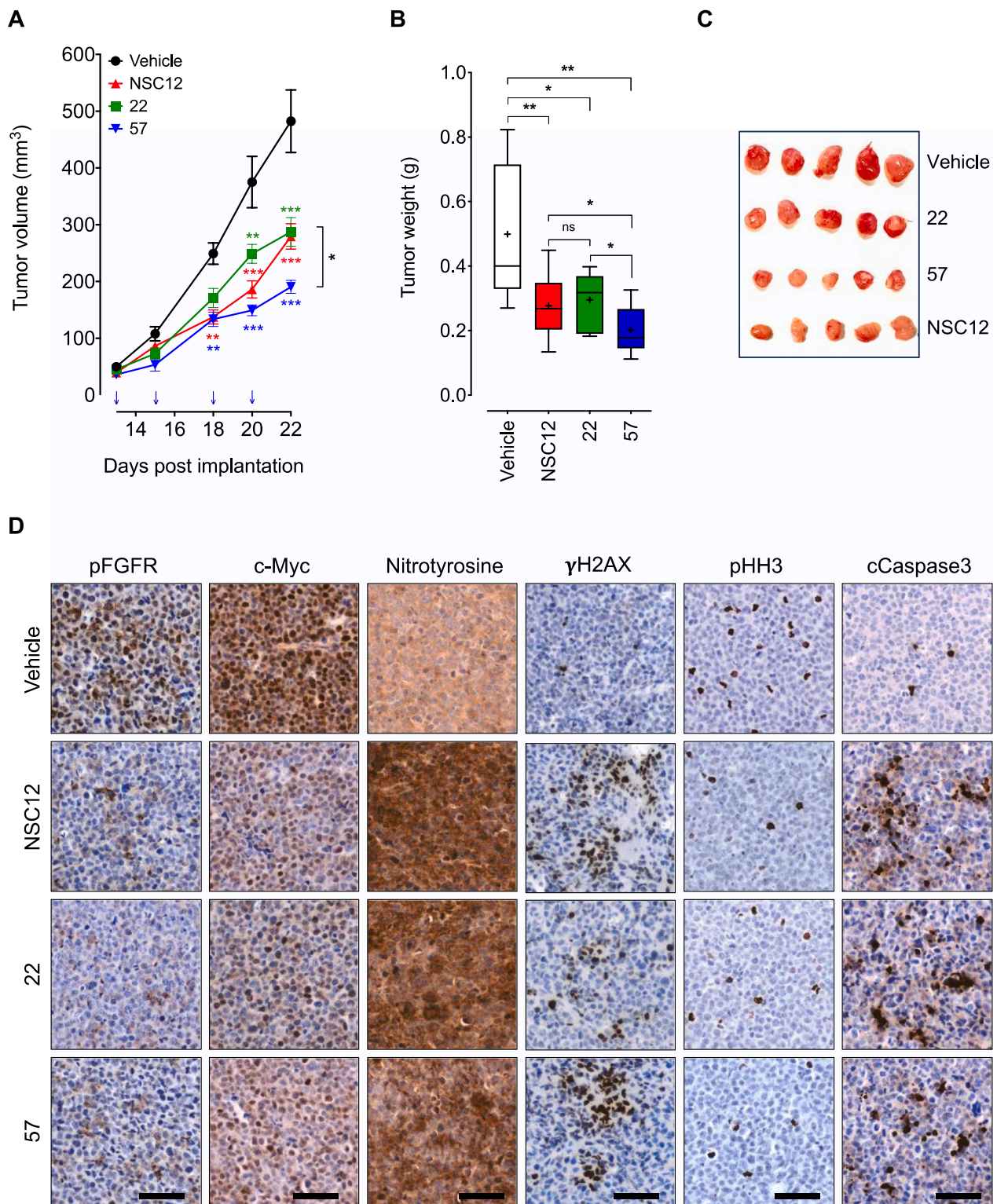


Fig. 7. NSC12 derivatives significantly reduced the growth of MM tumor xenografts in vivo. (A) Tumor growth in mice treated with vehicle (DMSO), NSC12, compound 22 or compound 57. Blue arrows indicate the day of treatment. (B) Weight of tumors from mice treated with vehicle, NSC12, compound 22 or compound 57. (C) Representative pictures of tumors reported in (B). (D) Immunohistochemical analysis of tumors shown in (C). Scale bar 50 μ m.

models and cancer patients, administration of NSC12 derivatives did not affect the blood levels of phosphorus and calcium (Figure S5B). This is in keeping with data previously obtained after in vivo treatment with NSC12 [11] or other FGF traps like FP-1039 [9].

Data are mean \pm SEM (n = at least 5 mice/group). In box and whiskers graphs, boxes extend from the 25th to the 75th percentiles,

lines indicate the median values, + indicates the mean values and whiskers indicate the range of values. * p<0.05, ** p<0.01, *** p<0.001.

3.5. Compounds 22 and 57 induce cell death in both newly diagnosed and relapsed/refractory patient-derived MM cells

To investigate the therapeutic potential of the identified non-steroidal NSC12 derivatives, the antitumor activity of compounds 22 and 57 was assessed on MM cells purified from both naïve and relapsed/refractory patients (Table S1). As shown in Table 2 and Fig. 8A, treatment with compounds 22 and 57 significantly induced cell death in primary MM cell cultures in a manner similar to that observed for NSC12 (1), whereas compound 59 was ineffective. Importantly, in keeping with the data obtained with bortezomib-sensitive and -resistant KMS-11 cells (see Fig. 5), similar antitumor effects were exerted by the two NSC12 derivatives on cells derived from both newly diagnosed and relapsed/refractory MM patients (Table 2 and Fig. 8A). In addition, Western blot analysis performed on MM cells purified from patient 2 confirmed the capacity of compounds 22 and 57 to efficiently inhibit FGFR phosphorylation and the lack of FGF trap activity for compound 59 (Fig. 8B). To note, as previously reported [41], treatment of peripheral blood mononuclear cells (PBMCs) from healthy donors with NSC12, compounds 22 or 57 did not exert a significant cytotoxic effect as shown by the absence of caspase 3 activation assessed by Western blot analysis (Figure S6).

Taken together these results indicate that non-steroidal NSC12 derivatives 22 and 57 might set the bases for the development of new therapeutic strategies for the treatment of naïve MM patients as well as for those patients that are not responsive or develop resistance to proteasome inhibitor regimens.

4. Discussion

We previously identified NSC12 (1) as the first orally available small molecule FGF trap able to inhibit the growth and progression of several FGF-dependent tumor models, including MM. NSC12 is a pregnenolone derivative carrying a 1,1-bis-trifluoromethyl-1,3-propanediol chain in position 17 of the steroid nucleus. SAR investigation highlighted that the C17-side chain, but not the steroid portion, is pivotal for the FGF trap activity [13]. Based on this evidence, here we applied a scaffold hopping approach to obtain NSC12-derived FGF trap compounds devoid of the steroid nucleus. The design of new compounds was based on the replacement of the tetracyclic scaffold of NSC12 (1) with simplified structures that could guarantee binding to FGFs and inhibition of FGFR activation while providing more opportunities for structural diversification and optimization given their higher synthetic accessibility. The 1,1-bis-trifluoromethyl-1,3-propanediol side chain of the lead NSC12 (1) was maintained since it is necessary for FGF binding [13].

Previous observations had shown that the FGF/FGFR signaling system is essential for survival and proliferation of MM cells [42] and that

Table 2

Percentage of cell death of primary MM cells purified from newly diagnosed (ND) and relapsed/refractory (R/R) patients and treated with NSC12 (1) or compounds 22, 57, and 59 for 12 hours at 10 μ M concentration. Data are mean \pm SEM (n = 3 replicates).

Pt.	DIAGNOSIS	CELL DEATH (%)				
		DMSO	NSC12	57	22	59
1	ND	16.2 \pm 0.3	43.8 \pm 3.9	50.8 \pm 4.1	48.5 \pm 2.5	21.8 \pm 0.6
		29.8 \pm 3.8	90.3 \pm 3.1	65.8 \pm 6.6	81.6 \pm 8.1	28.7 \pm 0.5
3	ND	33.5 \pm 1.1	57.1 \pm 1.2	71.1 \pm 4.4	68.8 \pm 0.2	43.4 \pm 1.0
		43.9 \pm 1.4	83.3 \pm 1.6	80.3 \pm 0.8	75.4 \pm 5.8	47.7 \pm 2.8
5	R/R	28.2 \pm 0.6	73.2 \pm 0.3	69.5 \pm 0.8	73.4 \pm 0.3	40.3 \pm 1.0
		34.1 \pm 0.8	81.4 \pm 2.7	57.8 \pm 1.2	68.4 \pm 1.6	34.8 \pm 0.9

the FGF trap NSC12 (1) is able to efficiently inhibit FGFR activation and to produce an oncosuppressive effect on MM cell lines and primary cells obtained from MM patients [41]. New compounds were therefore initially screened by evaluating their ability to inhibit FGFR3 phosphorylation in the MM KMS-11 cell line in which a t(4;14) chromosomal translocation leads to FGFR3 overexpression and autocrine FGF-dependent signaling hyperactivation [33]. The biphenyl and the β -(phenyl)-naphthyl scaffolds were selected as potential replacement for the steroid nucleus, given the successful reports in the field of estrogen receptor ligands [43,44]. Additionally, more flexible open-ring derivatives and conformationally constrained analogs were investigated. In fact, while flexible compounds can in principle allow a better fitting to the FGF surface, constrained analogs can provide higher potency due to enrichment of the biologically relevant conformation. Suitable scaffold decoration led to the most potent β -(phenyl)-naphthyl derivative 22, showing the same inhibitory activity as NSC12 (1), and to the phenoxymethyl derivative 26, also endowed with significant potency. Based on the mechanism of FGF traps as protein-protein interaction (PPI) inhibitors, which bind to the surface of FGF hampering the formation of the active HSPG/FGF/FGFR ternary complex, a further potency improvement was pursued by merging the structural features of the two most potent inhibitors (compounds 22 and 26) into one molecule (compound 57). In fact, PPI inhibitors are generally characterized by higher molecular weight than classical receptor- or enzyme-targeting drugs, allowing interactions with a larger surface of the host protein [45]. As assessed in SPR binding assay, compound 57 binds to FGF2 more tightly than parent compound 22, likely due to additional interactions brought by the second pharmacophore portion. The relevance of specific interactions undertaken by the lipophilic portion of FGF traps with the FGF counterpart was confirmed by the loss of affinity and efficacy shown by compound 59, in which the alkyl tail provides similar lipophilicity but no recognition elements.

From the translational point of view, our results demonstrate that compounds 22 and 57 are able to block FGFR activation in MM cells, thus inhibiting tumor cell growth and survival both *in vitro* and *in vivo*. Mechanistically, as previously described for NSC12 [41], compounds 22 and 57 induces the rapid proteasomal degradation of the oncoprotein c-Myc that is paralleled by mitochondrial oxidative stress, DNA damage and eventually apoptotic tumor cell death.

In vitro, a significant reduction of FGFR phosphorylation levels and antitumor effect were observed not only on several MM cell lines, but also in patient-derived MM cells. Of note, compounds 22 and 57 strongly affected the survival of both proteasome inhibitor-sensitive and -resistant MM cells, representing a potential therapeutic option for relapsed/refractory MM patients. In this context, in future studies it will be important to assess the therapeutic potential of the newly identified FGF traps in combination with first-line MM drugs, such as immunomodulatory drugs (IMiDs), daratumumab, melfalan or Proteasome Inhibitors (PIs). However, it is worth to mention that in previous studies we demonstrated that proteasome inhibition can substantially abrogate the effect exerted by FGF blockade on c-Myc degradation, which, in turn, is essential to induce MM cell death [41]. Thus, therapies based on the combination of FGF traps and PIs may show a limited therapeutic window. Rather than representing a possible supportive therapy in combination with PIs, FGF/FGFR blockade may set the basis for the development of promising second-/third line approaches to eradicate proteasome inhibitor-relapsed/refractory MM cells.

In vivo, both NSC12 derivatives exerted significant antitumor activity without any sign of toxicity and compound 57 exerted a better antitumor activity compared to compound 22 and NSC12. These *in vivo* experiments were performed by intraperitoneal treatments and by using subcutaneous MM models. Future studies will be required to assess the oral bioavailability and the effect of the novel FGF traps in systemic models of MM in mice and zebrafish embryos, as previously reported for NSC12 [41].

In conclusion, based on the findings here reported, we propose

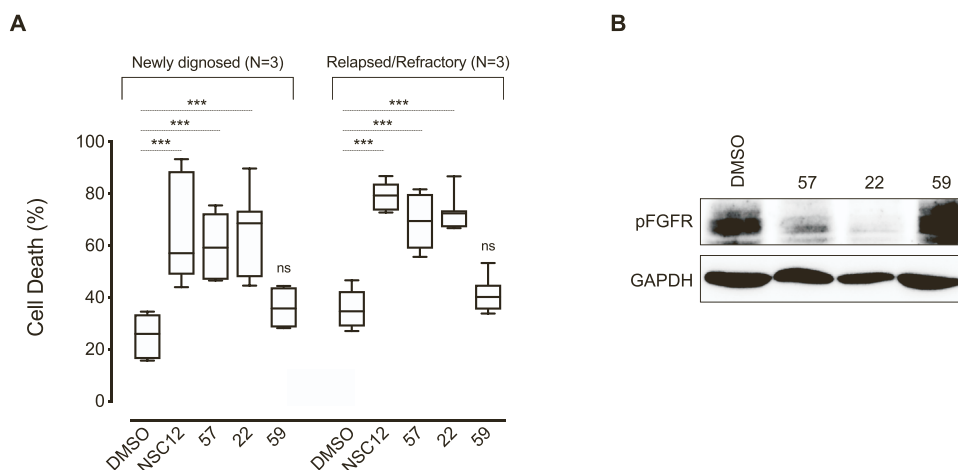


Fig. 8. NSC12 derivatives exert an oncosuppressive effect on patient-derived primary MM cells. (A) Quantification of cell death percentage by cytofluorimetric analysis after staining with propidium iodide. MM cells purified from newly diagnosed and relapsed/refractory patients ($N = 3$ / group) were treated with NSC12 (1) or compounds **22**, **57**, and **59** for 12 hours at $10 \mu\text{M}$ concentration. In box and whiskers graphs, boxes extend from the 25th to the 75th percentiles, lines indicate the median values, and whiskers indicate the range of values. # $p < 0.001$, ns = not significant. (B) Western blot analysis of MM cells purified from patient 2 after 6-hour treatment with non-steroidal derivatives **22**, **57** or **59** at $10 \mu\text{M}$ concentration. GAPDH was used as loading control.

compounds **22** and **57** as new non-steroidal NSC12 derivatives to set the bases for the development of novel FGF traps to be used in the clinic for the treatment of those tumors in which the FGF/FGFR system plays a pivotal role, including MM.

5. Methods

5.1. Chemistry

5.1.1. General methods

All chemicals were obtained from commercial suppliers and used without further purification. Solvents were purified and stored according to standard procedures. Anhydrous reactions were conducted under a positive pressure of anhydrous N_2 . Reactions were monitored by TLC, on Merck silica gel 60 F254 plates. Final compounds and intermediates were purified by column chromatography under “flash” conditions using Merck 230–400 mesh silica gel. Melting points were determined on a Buchi B-540 capillary melting point apparatus or on a Gallenkamp melting point apparatus and are uncorrected. ^1H NMR and ^{13}C NMR spectra were recorded on a Bruker AVANCE 300 MHz or 400 MHz instrument. Chemical shifts (δ scale) are reported in parts per million (ppm) relative to the central peak of the solvent. ESI-MS spectra of the final products were acquired on a Thermo TSQ Quantum Access Max triple quadrupole mass spectrometer (Thermo, San Jose, CA, USA) equipped with a heated electrospray ionization (H-ESI) source. The purity of tested compounds, determined by high performance liquid chromatography – mass spectrometry (HPLC-MS), was greater than 95 %.

5.1.2. Compound synthesis and characterization

5.1.2.1. General Procedure A. Suzuki-Miyaura coupling between an aryl boronic acid/boronate ester and an aryl halide. To a stirred solution of aryl halide (1 molar equivalent) and the aryl boronic acid/boronate ester (1.1 molar equivalent) in 1,4 dioxane (0.1 M), potassium carbonate (4.0 molar equivalent) and bis(triphenylphosphine) palladium dichloride (0.5 % mol) are added. The mixture is heated to reflux under nitrogen atmosphere for 3 h, then cooled to room temperature. The mixture is diluted with ethyl acetate and washed with water, HCl 1 M and brine. The organic layer is collected and dried over sodium sulfate, filtered and the solvent is removed under reduced pressure. The mixture is purified by silica gel column chromatography with the appropriate

solvent mixture.

5.1.2.2. General Procedure B: aldol condensation with hexafluoroacetone and reduction with sodium borohydride. Part i. To a stirred solution of methyl ketone at -60°C in anhydrous THF under nitrogen atmosphere, LiHMDS (1.0 M solution in THF, 1.3 molar equivalent) is added dropwise and stirred for 30 min. In a separate two neck flask, concentrated H_2SO_4 (15 ml) is warmed to 50°C and connected through a cannula with the flask containing the ketone-enolate. An argon overpressure is applied to the flask containing sulfuric acid, while the flask at -60°C is vented. HFA trihydrate (4 molar equivalent) is added dropwise to the warm sulfuric acid and the gaseous HFA thus formed is delivered by the stream of argon to the cold enolate solution. When all the HFA has been delivered, the reaction is allowed to warm to room temperature. The reaction is quenched with glacial acetic acid (1.3 molar equivalent). The mixture is diluted with ethyl acetate and washed with water and brine. The organic layer is collected and dried over sodium sulfate, filtered and the solvents removed under reduced pressure. The crude product is checked by ^1H -NMR spectroscopy.

Part ii. The crude material is dissolved in methanol (0.1 M), cooled to 0°C and NaBH_4 (2 molar equivalent) is then added. When the reaction is judged to be complete by TLC analysis, the reaction is quenched with glacial acetic acid, poured over water and extracted three times with ethyl acetate. The combined organic layers are dried over sodium sulfate, the solvent is removed under reduced pressure and the product is purified by silica gel column chromatography with the specified solvent mixture.

5.1.2.3. Ethyl 4'-formyl-[1,1'-biphenyl]-4-carboxylate (3). Following general procedure A, employing ethyl-4-iodo benzoate (1.00 g, 3.6 mmol) and 4-acetylphenyl boronic acid (605 mg, 4.0 mmol), product **3** (810 mg, 87 %) is obtained after silica gel column chromatography (petroleum ether/Ethyl acetate = 10/1) as a white solid. ^1H NMR (300 MHz, CDCl_3) δ 8.18 – 8.10 (m, 2 H), 8.10 – 8.01 (m, 2 H), 7.70 (dd, $J = 9.0, 7.4$ Hz, 4 H), 4.41 (q, $J = 7.1$ Hz, 2 H), 2.65 (s, 3 H), 1.42 (t, $J = 7.1$ Hz, 3 H).

5.1.2.4. Ethyl 4'-(4,4,4-trifluoro-3-hydroxy-3-(trifluoromethyl)butanoyl)-[1,1'-biphenyl]-4-carboxylate (4). Following general procedure B, part i, starting from methyl ketone **3** (300 mg, 1.1 mmol), β -hydroxy ketone **4** (462 mg, 95 %) is obtained as a white solid. ^1H NMR (300 MHz, CDCl_3) δ 8.21 – 8.12 (m, 2 H), 8.11 – 7.99 (m, 2 H), 7.83 – 7.74 (m, 2 H), 7.74 –

7.66 (m, 2 H), 7.12 (s, 1 H), 4.42 (q, $J = 7.1$ Hz, 2 H), 3.50 (s, 2 H), 1.43 (t, $J = 7.1$ Hz, 3 H).

5.1.2.5. Ethyl 4'-(4,4,4-trifluoro-1,3-dihydroxy-3-(trifluoromethyl)butyl)-[1,1'-biphenyl]-4-carboxylate (5). Following general procedure B, part ii, crude **4** (0.45 g, 1.1 mmol) is reduced and purified (petroleum ether/Ethyl acetate 10/1) to obtain **5** (340 mg, 75 %) as a white solid. ^1H NMR (400 MHz, CDCl_3) δ 8.01 – 7.97 (m, 2 H), 7.61 – 7.53 (m, 4 H), 7.46 – 7.42 (m, 2 H), 6.39 (bs, 1 H), 5.36 (d, $J = 11.4$ Hz, 1 H), 4.38 (q, $J = 7.1$ Hz, 2 H), 2.40 – 2.32 (m, 1 H), 2.27 – 2.12 (m, 1 H), 1.41 (t, $J = 7.1$ Hz, 3 H). ^{13}C NMR (100 MHz, CDCl_3) δ 167.0, 144.7, 142.3, 140.6, 130.2, 129.5, 128.0, 127.1, 126.2, 123.7 (q, $J = 286$ Hz), 122.8 (q, $J = 284$ Hz) 76.6 (m), 71.7, 61.4, 36.4, 14.4. HPLC-MS (ESI): calcd for $\text{C}_{20}\text{H}_{18}\text{F}_6\text{O}_4$: 436.11; found m/z : 435.28 [M-H] $^-$.

5.1.2.6. 4'-(4,4,4-trifluoro-1,3-dihydroxy-3-(trifluoromethyl)butyl)-[1,1'-biphenyl]-4-carboxylic acid (6). Compound **5** (0.3 g, 0.7 mmol) is dissolved in THF (5 ml) and a solution of NaOH (90 mg, 2.1 mmol) in water (50 ml) is added. The reaction is stirred at room temperature for 16 h. The mixture is diluted with HCl 1 M and washed with ethyl acetate. The organic layer is collected and dried over sodium sulfate. After filtration, the solvents are removed under reduced pressure. Purification by silica gel column chromatography (DCM + 1 % AcOH) affords **6** (200 mg, 70 %) as a white solid. ^1H NMR (300 MHz, $\text{DMSO}-d_6$) δ 12.94 (s, 1 H), 8.02 (d, $J = 8.3$ Hz, 2 H), 7.83 – 7.69 (m, 4 H), 7.51 (d, $J = 8.1$ Hz, 2 H), 6.41 (d, $J = 5.1$ Hz, 1 H), 5.09 (d, $J = 9.3$ Hz, 1 H), 2.37 – 2.10 (m, 2 H). ^{13}C NMR (100 MHz, $\text{DMSO}-d_6$) δ 167.2, 144.9, 144.0, 138.3, 131.6, 129.6, 127.0, 126.8, 126.5, 123.6 (q, $J = 286$ Hz), 123.1 (q, $J = 284$ Hz), 75.7 (m), 67.8, 37.8. HPLC-MS (ESI): calcd for $\text{C}_{18}\text{H}_{14}\text{F}_6\text{O}_4$: 408.08; found m/z : 407.37 [M-H] $^-$.

5.1.2.7. 4,4,4-trifluoro-1-(4'-(hydroxymethyl)-[1,1'-biphenyl]-4-yl)-3-(trifluoromethyl)butane-1,3-diol (7). Compound **4** (0.45 g, 1.1 mmol) is dissolved in THF (15 ml) at 0 °C under nitrogen atmosphere. Lithium aluminium hydride (1.0 M in THF, 2.1 ml, 2.1 mmol) is added dropwise. When the reaction is complete as judged by TLC analysis, the reaction is quenched by the addition of Ethyl acetate (50 ml). The mixture is poured over an aqueous solution of sodium potassium tartrate and the organic layer is separated, washed with an aqueous saturated solution of NaHCO_3 and brine. The organic layer is collected and dried over sodium sulfate. After filtration, the solvents are removed under reduced pressure. Purification by silica gel column chromatography (petroleum ether/Ethyl acetate = 10/1) affords **7** (248 mg, 58 %) as a white solid. ^1H NMR (400 MHz, CDCl_3) δ 7.65 – 7.54 (m, 4 H), 7.44 (d, $J = 7.8$ Hz, 4 H), 6.19 (s, 1 H), 5.35 (d, $J = 11.5$ Hz, 1 H), 4.75 (s, 2 H), 2.48 – 2.37 (m, 1 H), 2.25 (d, $J = 15.5$ Hz, 1 H). ^{13}C NMR (100 MHz, $\text{CD}_3\text{OD}/\text{CDCl}_3$) δ 142.4, 140.9, 140.5, 139.8, 127.6, 127.4, 127.2, 126.0, 123.9 (q, $J = 286$ Hz), 123.0 (q, $J = 284$ Hz), 76.7 (m), 70.4, 64.3, 36.3. HPLC-MS (ESI): calcd for $\text{C}_{18}\text{H}_{16}\text{F}_6\text{O}_3$: 394.10; found m/z : 393.41 [M-H] $^-$.

5.1.2.8. Ethyl 3'-acetyl-[1,1'-biphenyl]-4-carboxylate (8). Following general procedure A, employing ethyl-4-iodo benzoate (500 mg, 1.8 mmol) and 3-acetylphenyl boronic acid (320 mg 2.0 mmol), product **8** (403 mg, 83 %) is obtained after silica gel column chromatography (petroleum ether/Ethyl acetate 10/1) as a white solid. ^1H NMR (400 MHz, CDCl_3) δ 8.21 (t, $J = 1.8$ Hz, 1 H), 8.17 – 8.11 (m, 2 H), 7.98 (dt, $J = 7.8, 1.4$ Hz, 1 H), 7.82 (ddd, $J = 7.7, 1.9, 1.1$ Hz, 1 H), 7.72 – 7.66 (m, 2 H), 7.58 (t, $J = 7.7$ Hz, 1 H), 4.42 (q, $J = 7.1$ Hz, 2 H), 2.67 (s, 3 H), 1.43 (t, $J = 7.1$ Hz, 3 H).

5.1.2.9. Ethyl 3'-(4,4,4-trifluoro-3-hydroxy-3-(trifluoromethyl) butanoyl)-[1,1'-biphenyl]-4-carboxylate (9). Following general procedure B, part i, starting from methyl ketone **8** (380 mg, 1.4 mmol), β -hydroxy ketone **9** (350 mg 58 %) is obtained as a white solid. ^1H NMR (300 MHz, CDCl_3) δ 8.22 – 8.12 (m, 3 H), 7.95 (tdd, $J = 7.8, 2.3, 1.2$ Hz, 2 H), 7.72 – 7.56 (m,

3 H), 7.04 (s, 1 H), 4.42 (q, $J = 7.1$ Hz, 2 H), 3.52 (s, 2 H), 1.43 (t, $J = 7.1$ Hz, 3 H).

5.1.2.10. Ethyl 3'-(4,4,4-trifluoro-1,3-dihydroxy-3-(trifluoromethyl) butyl)-[1,1'-biphenyl]-4-carboxylate (10). Following general procedure B, part ii, crude **9** (170 mg g, 0.4 mmol) is reduced and purified (petroleum ether/Ethyl acetate = 10/1) to obtain **10** (157 mg, quant.) as a white solid. ^1H NMR (400 MHz, CDCl_3) δ 8.14 – 8.06 (m, 2 H), 7.68 – 7.56 (m, 4 H), 7.51 (dd, $J = 8.8, 7.1$ Hz, 1 H), 7.40 (dt, $J = 7.7, 1.6$ Hz, 1 H), 6.20 (s, 1 H), 5.39 (d, $J = 11.4$ Hz, 1 H), 4.40 (q, $J = 7.1$ Hz, 2 H), 2.91 (s, 1 H), 2.43 (ddd, $J = 15.6, 11.5, 2.1$ Hz, 1 H), 2.26 (d, $J = 15.4$ Hz, 1 H), 1.41 (t, $J = 7.1$ Hz, 3 H). ^{13}C NMR (100 MHz, CDCl_3) δ 166.8, 144.9, 143.1, 141.0, 130.3, 129.8, 127.9, 127.2, 125.3, 123.7 (q, $J = 286$ Hz), 122.8 (q, $J = 284$ Hz), 76.6 (m), 72.0, 61.4, 36.6, 14.4. HPLC-MS (ESI): calcd for $\text{C}_{20}\text{H}_{18}\text{F}_6\text{O}_4$: 436.11; found m/z : 435.11 [M-H] $^-$.

5.1.2.11. 3'-(4,4,4-Trifluoro-1,3-dihydroxy-3-(trifluoromethyl)butyl)-[1,1'-biphenyl]-4-carboxylic acid (11). Compound **10** (111 mg g, 0.2 mmol) is dissolved in THF (3 ml) and a solution of NaOH (70 mg, 1.7 mmol) in water (20 ml) is added. The reaction is stirred at room temperature for 16 h. The mixture is diluted with HCl 1 M and washed with ethyl acetate. The organic layer is collected and dried over sodium sulfate. After filtration, the solvents are removed under reduced pressure. Purification by silica gel column chromatography (DCM + 1 % AcOH) affords **11** (62 mg, 73 %) as a white solid. ^1H NMR (400 MHz, CD_3OD) δ 8.14 – 8.08 (m, 2 H), 7.78 – 7.72 (m, 2 H), 7.69 (d, $J = 1.9$ Hz, 1 H), 7.64 (dt, $J = 7.6, 1.5$ Hz, 1 H), 7.50 (t, $J = 7.7$ Hz, 1 H), 7.42 (dt, $J = 7.7, 1.5$ Hz, 1 H), 5.30 – 5.23 (m, 1 H), 2.39 – 2.19 (m, 2 H). ^{13}C NMR (100 MHz, CD_3OD) δ 169.7, 146.6, 146.1, 141.8, 131.4, 130.5, 128.1, 128.0, 126.4, 125.3 (q, $J = 287$ Hz), 124.4 (q, $J = 284$ Hz), 77.8 (m), 71.3, 38.0. HPLC-MS (ESI): calcd for $\text{C}_{18}\text{H}_{14}\text{F}_6\text{O}_4$: 408.08; found m/z : 407.07 [M-H] $^-$.

5.1.2.12. 4,4,4-Trifluoro-1-(4'-(hydroxymethyl)-[1,1'-biphenyl]-3-yl)-3-(trifluoromethyl)butane-1,3-diol (12). Compound **9** (173 mg, 0.4 mmol) is dissolved in THF (15 ml) at 0 °C under nitrogen atmosphere. Lithium aluminium hydride (1.0 M in THF, 0.8 ml, 0.8 mmol) is added dropwise. When the reaction is complete as judged by TLC analysis, the reaction is quenched by the addition of ethyl acetate (50 ml). The mixture is poured over an aqueous solution of sodium potassium tartrate and the organic layer is separated, washed with an aqueous saturated solution of NaHCO_3 and brine. The organic layer is dried over sodium sulfate. After filtration, the solvents are removed under reduced pressure. Purification by silica gel column chromatography (petroleum ether/ethyl acetate = 10/1) affords compound **12** (110 mg, 70 %) as a white solid. ^1H NMR (300 MHz, CD_3OD) δ 7.65 – 7.52 (m, 4 H), 7.45 (t, $J = 7.6$ Hz, 3 H), 7.35 (dt, $J = 7.6, 1.5$ Hz, 1 H), 5.29 – 5.20 (m, 1 H), 4.65 (s, 2 H), 2.33 (ddd, $J = 15.1, 10.6, 1.9$ Hz, 1 H), 2.22 (dd, $J = 15.3, 2.8$ Hz, 1 H). ^{13}C NMR (100 MHz, CD_3OD) δ 145.8, 142.7, 142.1, 141.2, 130.3, 128.6, 128.0, 127.7, 125.5, 125.2 (q, $J = 286$ Hz), 125.0, 124.4 (q, $J = 284$ Hz), 77.8 (m), 71.4, 64.9, 38.0. HPLC-MS (ESI): calcd for $\text{C}_{18}\text{H}_{16}\text{F}_6\text{O}_3$: 394.10; found m/z : 393.12 [M-H] $^-$.

5.1.2.13. 1-(4-Bromophenyl)-4,4,4-trifluoro-3-(trifluoromethyl)butane-1,3-diol (13). Following general procedure B, starting from 4-bromo acetophenone (1.51 g, 7.5 mmol), **13** (1.61 g, quant.) is obtained after silica gel column chromatography (petroleum ether/ethyl acetate = 10/1) as colorless oil. ^1H NMR (400 MHz, CDCl_3) δ 7.59 – 7.52 (m, 2 H), 7.29 – 7.24 (m, 2 H), 6.29 (s, 1 H), 5.27 (d, $J = 11.5$ Hz, 1 H), 3.38 (t, $J = 2.4$ Hz, 1 H), 2.33 (ddq, $J = 15.7, 11.6, 2.1$ Hz, 1 H), 2.18 (d, $J = 15.4$ Hz, 1 H).

5.1.2.14. 1-(4-Bromophenyl)-4,4,4-trifluoro-3-hydroxy-3-(trifluoromethyl)butyl (tert-butoxycarbonyl)-L-alaninate (14a,b). Compound

13 (463 mg, 1.3 mmol), *N*-(*t*-butoxycarbonyl)-L-alanine (811 mg, 1.6 mmol) and DMAP (40 mg, 0.35 mmol) are dissolved in DCM (20 ml) and cooled to 0 °C. EDCl (378 mg, 2.0 mmol) is added, and the mixture is stirred under nitrogen atmosphere at room temperature for 18 h. The mixture is diluted with DCM and washed with water, NaHCO₃ and brine. The organic layer is separated and dried over sodium sulfate, filtered and the solvent is removed under reduced pressure. The mixture is purified by silica gel column chromatography (toluene/ethyl acetate 10/1) to afford **14a** (250 mg, 36 %) and **14b** (80 mg, 11 %) as white foams. **14a**: ¹H NMR (300 MHz, CDCl₃) δ 7.56–7.47 (m, 2 H), 7.31–7.10 (m, 2 H), 6.08 (d, *J* = 10.1 Hz, 1 H), 5.32 (s, 1 H), 4.91 (d, *J* = 6.0 Hz, 1 H), 4.19 (p, *J* = 7.1 Hz, 1 H), 2.71–2.56 (m, 1 H), 2.32 (d, *J* = 17.0 Hz, 1 H), 1.43 (s, 9 H), 1.29 (d, *J* = 7.1 Hz, 3 H). **14b**: ¹H NMR (400 MHz, CDCl₃) δ 7.58–7.51 (m, 2 H), 7.33–7.15 (m, 2 H), 6.17 (d, *J* = 10.3 Hz, 1 H), 5.46 (s, 1 H), 4.93 (d, *J* = 7.1 Hz, 1 H), 4.31 (t, *J* = 7.2 Hz, 1 H), 2.66–2.53 (m, 1 H), 2.35 (d, *J* = 16.1 Hz, 1 H), 1.49 (s, 9 H), 1.41 (d, *J* = 7.2 Hz, 3 H).

5.1.2.15. 1-(4-Bromophenyl)-4,4,4-trifluoro-3-(trifluoromethyl)butane-1,3-diol (15a). Compound **14a** (248 mg, 0.5 mmol) is dissolved in methanol (10 ml). The solution is cooled at 0 °C under nitrogen atmosphere and freshly cut sodium (35 mg, 1.5 mmol) is added. The reaction is stirred and allowed to warm to room temperature over the course of 24 h, then is quenched with glacial acetic acid, diluted with dichloromethane and washed with HCl 1 M and brine. The organic layer is collected and dried over sodium sulfate, filtered and the solvent was evaporated under reduced pressure. The product is purified with silica gel column chromatography (petroleum ether/Et₂O = 10/1) to afford **15a** (153 mg, 82 %) as a colorless oil. See compound **13** for ¹H NMR.

5.1.2.16. 1-(4-Bromophenyl)-4,4,4-trifluoro-3-(trifluoromethyl)butane-1,3-diol (15b). Following the same procedure for **15a**, starting from **14b** (85 mg, 0.2 mmol), **15b** (petroleum ether/Et₂O = 10/1) is obtained as colourless oil (50 mg, 91 %). See compound **13** for ¹H NMR.

5.1.2.17. Ethyl 4'-(4,4,4-trifluoro-1,3-dihydroxy-3-(trifluoromethyl)butyl)-[1,1'-biphenyl]-4-carboxylate (16 -). Following general procedure A, starting from (**15a**) (100 mg, 0.3 mmol) and 4-(ethoxycarbonyl)phenylboronic acid (**18**, 62 mg, 0.3 mmol) **16** (90 mg, 69 %) is obtained after silica gel column chromatography (petroleum ether/Et₂O = 10/1) as a white solid. [α]_D²⁰ = -41.8 (*c* = 4.35 mg/ml, CHCl₃). See compound **5** for ¹H NMR and ¹³C NMR. HPLC-MS (ESI): calcd for C₂₀H₁₈F₆O₄: 436.11; found *m/z*: 435.15 [M-H]⁻.

5.1.2.18. Ethyl 4'-(4,4,4-trifluoro-1,3-dihydroxy-3-(trifluoromethyl)butyl)-[1,1'-biphenyl]-4-carboxylate (17 +). Following general procedure A, starting from (**15b**) (50 mg, 0.1 mmol) and 4-(ethoxycarbonyl)phenylboronic acid (**18**, 30 mg, 0.2 mmol), **17** (20 mg, 35 %) is obtained after silica gel column chromatography (petroleum ether/Et₂O = 10/1) as a white solid. See compound **5** for ¹H NMR and ¹³C NMR. HPLC-MS (ESI): calcd for C₂₀H₁₈F₆O₄: 436.11; found *m/z*: 435.14 [M-H]⁻.

5.1.2.19. ((6-Bromonaphthalen-2-yl)oxy)(tert-butyl)dimethylsilane (20). 6-Bromonaphthol **19** (1.0 g, 4.5 mmol) and (*tert*-butyl)dimethylsilyl chloride (802 mg, 5.5 mmol) are placed in degassed DMF at 0 °C and triethyl amine (1.0 ml, 6.5 mmol) is added. The reaction is stirred 24 h, then is diluted with ethyl acetate and washed with water and brine. The organic layer is collected and dried over sodium sulfate, filtered and the solvent is removed under reduced pressure. The residue is purified by silica gel column chromatography (petroleum ether) to afford **20** (1.0 g, 66 %) as a white solid. ¹H NMR (300 MHz, CDCl₃) δ 7.96–7.86 (m, 1 H), 7.68–7.43 (m, 3 H), 7.19–7.04 (m, 2 H), 1.02 (s, 9 H), 0.25 (s, 6 H).

5.1.2.20. 1-(4-(6-((Tert-butyl)dimethylsilyloxy)naphthalen-2-yl)phenyl)ethan-1-one (21). Following general procedure A, starting from **20** (398 mg, 1.2 mmol) and 4-acetyl-phenylboronic acid pinacol ester (352 mg, 1.4 mmol), **21** (300 mg, 66 %) is obtained after silica gel column chromatography (toluene/hexane = 10/3) as a white solid. ¹H NMR (300 MHz, CDCl₃) δ 8.15–7.97 (m, 3 H), 7.80 (dd, *J* = 8.6, 3.2 Hz, 4 H), 7.71 (dd, *J* = 8.6, 1.8 Hz, 1 H), 7.24–7.08 (m, 2 H), 2.66 (s, 3 H), 1.03 (s, 9 H), 0.27 (s, 6 H).

5.1.2.21. 4,4,4-Trifluoro-1-(4-(6-hydroxynaphthalen-2-yl)phenyl)-3-(trifluoromethyl)butane-1,3-diol (22). Following general procedure B, part i, starting from compound **21** (250 mg, 0.7 mmol) the product **22** (241 mg, 96 %) is obtained as a white solid. The intermediate β-hydroxy ketone is checked by ¹H NMR (300 MHz, CDCl₃) δ 7.95 (d, *J* = 1.9 Hz, 1 H), 7.83–7.62 (m, 5 H), 7.47 (d, *J* = 8.3 Hz, 2 H), 7.22 (d, *J* = 2.3 Hz, 1 H), 7.12 (dd, *J* = 8.8, 2.4 Hz, 1 H), 6.26 (s, 1 H), 5.41–5.31 (m, 1 H), 2.44 (ddd, *J* = 15.5, 11.5, 2.1 Hz, 1 H), 2.32–2.21 (m, 1 H), 1.04 (s, 9 H), 0.27 (s, 6 H). This material (205 mg, 0.33 mmol) and TBAF (1.0 M solution in THF, 400 μl, 0.40 mmol) are dissolved in THF (10 ml) and stirred at room temperature for 3 h. The mixture is then diluted with ethyl acetate and washed with HCl 1 M and brine. The organic layer is collected and dried over sodium sulfate, filtered and the solvent is removed under reduced pressure. The crude product is purified by silica gel column chromatography (hexane/ethyl acetate = 1/1) to afford **22** (122 mg, 85 %) as a white solid. ¹H NMR (400 MHz, DMSO-*d*₆) δ 9.81 (s, 1 H), 8.07 (s, 1 H), 7.93–7.64 (m, 5 H), 7.49 (d, *J* = 8.1 Hz, 2 H), 7.17–7.06 (m, 2 H), 6.44 (bs, 1 H), 5.09 (d, *J* = 9.9 Hz, 1 H), 2.38–2.24 (m, 1 H), 2.19 (d, *J* = 15.1 Hz, 1 H). ¹³C NMR (100 MHz, DMSO-*d*₆) δ 143.5, 139.6, 134.0, 133.9, 129.9, 128.0, 126.8, 126.6, 126.4, 125.2, 125.1, 124.8 (q, *J* = 286 Hz), 123.1 (q, *J* = 284 Hz), 119.1, 108.5, 75.7 (m), 68.1, 37.7. HPLC-MS (ESI): calcd for C₂₁H₁₆F₆O₃: 429.09; found *m/z*: 429.25 [M-H]⁻.

5.1.2.22. 1-(3-(6-((Tert-butyl)dimethylsilyloxy)naphthalen-2-yl)phenyl)ethan-1-one (23). Following general procedure A, starting from **20** (498 mg, 1.5 mmol), 3-acetylphenyl boronic acid (311 mg, 1.8 mmol), **23** (350 mg, 62 %) is obtained as a white solid. ¹H NMR (400 MHz, CDCl₃) δ 8.29 (t, *J* = 1.8 Hz, 1 H), 8.03–7.99 (m, 1 H), 7.92 (dddd, *J* = 17.9, 7.8, 2.3, 1.2 Hz, 2 H), 7.80 (dd, *J* = 8.7, 3.5 Hz, 2 H), 7.71 (dd, *J* = 8.6, 1.9 Hz, 1 H), 7.57 (t, *J* = 7.7 Hz, 1 H), 7.23 (d, *J* = 2.4 Hz, 1 H), 7.13 (dd, *J* = 8.8, 2.4 Hz, 1 H), 2.69 (s, 3 H), 1.04 (s, 9 H), 0.27 (s, 6 H).

5.1.2.23. 4,4,4-trifluoro-1-(3-(6-hydroxynaphthalen-2-yl)phenyl)-3-(trifluoromethyl)butane-1,3-diol (24). Following general procedure B, starting from **23** (347 mg, 0.9 mmol), the intermediate product is obtained as a white solid (70 mg, 26 %). ¹H NMR (400 MHz, CDCl₃) δ 7.97–7.92 (m, 1 H), 7.79 (dd, *J* = 8.7, 4.5 Hz, 2 H), 7.71–7.62 (m, 3 H), 7.50 (t, *J* = 7.7 Hz, 1 H), 7.35 (dt, *J* = 7.6, 1.5 Hz, 1 H), 7.23 (d, *J* = 2.4 Hz, 1 H), 7.12 (dd, *J* = 8.8, 2.4 Hz, 1 H), 6.39–6.35 (m, 1 H), 3.03 (s, 1 H), 2.45 (dddd, *J* = 13.7, 11.5, 4.1, 2.0 Hz, 1 H), 2.32–2.22 (m, 1 H), 1.05 (s, 9 H), 0.28 (s, 6 H). The crude material (65 mg, 0.12 mmol) and TBAF (1.0 M solution in THF, 200 μl 0.2 mmol) are dissolved in THF and stirred at room temperature for 3 h. The mixture is then diluted with ethyl acetate and washed with HCl 1 M and brine. The organic layer is collected and dried over sodium sulfate, filtered and the solvent is removed under reduced pressure. The crude product is purified by silica gel column chromatography (toluene/Et₂O = 10/1) to afford **24** (50 mg, 97 %) as a white solid. ¹H NMR (400 MHz, CDCl₃) δ 7.96 (bs, 1 H), 7.79 (dd, *J* = 15.9, 8.7 Hz, 2 H), 7.73–7.64 (m, 3 H), 7.57–7.45 (m, 1 H), 7.36 (dt, *J* = 7.7, 1.5 Hz, 1 H), 7.21–7.09 (m, 2 H), 6.28 (s, 1 H), 5.39 (d, *J* = 11.4 Hz, 1 H), 2.91 (s, 1 H), 2.46 (m, 1 H), 2.29 (m, 1 H). ¹³C NMR (100 MHz, CDCl₃) δ 153.9, 142.8, 142.3, 135.7, 134.1, 130.4, 129.8, 129.2, 127.9, 127.3, 126.1, 126.0, 124.4, 124.3, 123.7 (q, *J* = 286 Hz), 122.8 (q, *J* = 284 Hz), 118.6, 109.5, 76.6 (m), 72.3, 36.6. HPLC-MS (ESI): calcd for C₂₁H₁₆F₆O₃: 430.10; found *m/z*: 429.16 [M-

H]`.

5.1.2.24. 1-(3-((4-Fluorophenoxy)methyl)phenyl)ethan-1-one (25). To a solution of 3-(bromomethyl)-acetophenone (788 mg, 3.7 mmol) and 4-fluorophenol (471 mg, 4.2 mmol) in degassed DMF (40 ml), potassium carbonate (1.0 g, 7.2 mmol) is added. The mixture is stirred at room temperature for 15 h, then poured over water and the mixture is extracted three times with ethyl acetate. The combined organic layers are washed with water, brine, collected and dried over sodium sulfate. The solvents are removed under reduced pressure and the residue is purified by silica gel column chromatography (DCM/petroleum ether = 1/1) to afford the product **25** (748 mg, 83 %) as a yellowish solid. ¹H NMR (400 MHz, CDCl₃) δ 8.02 (t, *J* = 2.1 Hz, 1 H), 7.92 (dt, *J* = 7.7, 1.5 Hz, 1 H), 7.67 – 7.60 (m, 1 H), 7.49 (t, *J* = 7.7 Hz, 1 H), 7.04 – 6.86 (m, 4 H), 5.08 (s, 2 H), 2.62 (s, 3 H).

5.1.2.25. 4,4,4-Trifluoro-1-(3-((4-fluorophenoxy) methyl) phenyl)-3-(trifluoromethyl)butane-1,3-diol (26). Following general procedure B, starting from **25** (748 mg, 3.01 mmol) the product is purified by column chromatography (DCM/petroleum ether = 1/1) to give **26** (707 mg, 61 %) as a white solid. ¹H NMR (400 MHz, CDCl₃) δ 7.54 – 7.32 (m, 4 H), 7.08 – 6.88 (m, 4 H), 6.13 (s, 1 H), 5.34 (d, *J* = 11.4 Hz, 1 H), 5.06 (s, 2 H), 2.41 (ddq, *J* = 15.6, 11.5, 2.1 Hz, 1 H), 2.24 (dd, *J* = 15.6, 2.2 Hz, 1 H); ¹³C NMR (100 MHz, CDCl₃) δ 157.7 (d, *J* = 235 Hz), 154.8, 142.7, 138.0, 129.5, 128.2, 125.4, 124.7123.6 (q, *J* = 284 Hz), 122.7 (q, *J* = 284 Hz), 116.1 (d, *J* = 12 Hz), 116.0 (d, *J* = 3 Hz), 76.6 (m), 72.0, 70.5, 36.5; HPLC-MS (ESI): calcd for C₁₈H₁₅F₇O₃: 412.09; found *m/z*: 411.00 [M-H]⁺.

5.1.2.26. 1-(4-((4-Fluorophenoxy)methyl)phenyl)ethan-1-one (27). To a solution of 4-(bromomethyl)-acetophenone (780 mg, 3.7 mmol) and 4-fluorophenol (469 mg, 4.2 mmol) in degassed DMF (40 ml), potassium carbonate (1.1 g, 7.2 mmol) is added. The mixture is stirred at room temperature for 15 h, then poured over water and the mixture is extracted three times with ethyl acetate. The combined organic layers are washed with water, brine, collected and dried over sodium sulfate. The solvents are removed under reduced pressure and the residue is purified by silica gel column chromatography (DCM/petroleum ether = 1/1) to afford the product **27** (723 mg, 80 %) as a yellowish solid. ¹H NMR (400 MHz, CDCl₃) δ 7.98 (d, *J* = 8.1 Hz, 2 H), 7.52 (d, *J* = 8.0 Hz, 2 H), 6.98 (t, *J* = 8.6 Hz, 2 H), 6.90 (dd, *J* = 9.2, 4.3 Hz, 2 H), 5.10 (s, 2 H), 2.61 (s, 3 H).

5.1.2.27. 4,4,4-Trifluoro-1-(4-((4-fluorophenoxy) methyl) phenyl)-3-(trifluoromethyl) butane-1,3-diol (28). Following general procedure B, starting from **27** (723 mg, 3.01 mmol) the product is purified by column chromatography (DCM/petroleum ether = 1/1) to give **28** (806 mg, 65 %) as a white solid. ¹H NMR (400 MHz, CDCl₃) δ 7.47 (d, *J* = 7.9 Hz, 2 H), 7.40 (d, *J* = 8.0 Hz, 2 H), 6.98 (t, *J* = 8.6 Hz, 2 H), 6.89 (dd, *J* = 9.2, 4.2 Hz, 2 H), 6.10 (s, 1 H), 5.32 (d, *J* = 11.5 Hz, 1 H), 5.04 (s, 2 H), 2.56 (s, 1 H), 2.44 – 2.32 (m, 1 H), 2.21 (d, *J* = 15.5 Hz, 1 H). ¹³C NMR (100 MHz, CDCl₃) δ 157.7 (d, *J* = 235 Hz), 154.7, 142.1, 137.8, 128.3, 125.9, 123.7 (q, *J* = 286 Hz), 122.7 (q, *J* = 284 Hz), 116.1 (d, *J* = 15 Hz), 116.0 (d, *J* = 4 Hz), 76.6 (m), 71.8, 70.3, 36.4. HPLC-MS (ESI): calcd for C₁₈H₁₅F₇O₃: 412.09; found *m/z*: 411.34 [M-H]⁺.

5.1.2.28. 3-((4-Fluorophenoxy)methyl)-4-methoxybenzaldehyde (30). 3-(Chloromethyl)-4-methoxybenzaldehyde **29** (500 mg, 2.71 mmol) and 4-fluoro phenol (0.32 g, 2.85 mmol) are dissolved in degassed DMF (30 ml) and potassium carbonate (0.70 g, 5.07 mmol) and potassium iodide (110 mg, 0.66 mmol) are added. The solution is stirred at room temperature for 18 h. The solution is diluted with water and extracted with DCM. The organic layer is collected and dried over sodium sulfate, filtered and the solvent is removed under reduced pressure. The crude product is purified with silica gel column chromatography (hexane/

ethyl acetate = 10/2) to afford **30** (362 mg, 65 %) as colorless oil. ¹H NMR (300 MHz, CDCl₃) δ 10.93 (s, 1 H), 9.06 (d, *J* = 2.2 Hz, 1 H), 8.88 (dd, *J* = 8.5, 2.2 Hz, 1 H), 8.15 – 7.86 (m, 5 H), 6.10 (s, 2 H), 4.98 (s, 3 H).

5.1.2.29. 4,4,4-Trifluoro-1-(3-((4-fluorophenoxy)methyl)-4-methoxyphenyl)-3-(trifluoromethyl)butane-1,3-diol (31). A solution of 2-(bromomethyl)-1,1,1,3,3,3-hexafluoropropan-2-ol (460 ml, 2.88 mmol) in anhydrous THF (10 ml) is cooled at –78 °C under argon. *n*-Butyllithium (1.6 M in THF, 3.8 ml, 6.05 mmol) is added dropwise at –78 °C under nitrogen atmosphere. The solution is stirred for 30 min, then a solution of **30** (250 mg, 0.96 mmol) in THF (5 ml) is added dropwise. The reaction is stirred at –78 °C under nitrogen atmosphere for additional 30 min, warmed to –30 °C and then quenched by the addition of acetic acid. The crude product is dissolved in DCM and washed with sodium bicarbonate solution. The organic layer is dried over sodium sulfate, filtered and the solvent is removed under reduced pressure. The crude product is purified with silica gel column chromatography (hexane/ethyl acetate = 5/1) to afford **31** (150 mg, 35 %) as a colorless oil. ¹H NMR (400 MHz, CDCl₃) δ 7.46 (d, *J* = 2.3 Hz, 1 H), 7.35 – 7.26 (m, 2 H), 7.07 – 6.88 (m, 4 H), 5.06 (s, 2 H), 3.88 (s, 3 H), 2.55 (q, *J* = 2.1 Hz, 1 H), 2.37 (ddd, *J* = 15.5, 11.4, 2.1 Hz, 1 H), 2.16 (d, *J* = 15.4 Hz, 1 H). ¹³C NMR (100 MHz, CDCl₃) δ 157.6 (d, *J* = 237 Hz), 157.3, 154.9, 134.4, 126.5, 126.1, 125.9, 123.7 (q, *J* = 286 Hz), 122.8 (q, *J* = 284 Hz), 116.1 (d, *J* = 2 Hz), 116.0 (d, *J* = 32 Hz), 115.9, 110.8, 76.5 (m), 71.5, 65.8, 55.8, 36.3. HPLC-MS (ESI): calcd for C₁₉H₁₇F₇O₄: 441.09; found *m/z*: 441.01 [M-H]⁺.

5.1.2.30. 3-((4-Chlorophenoxy)methyl)-4-methoxybenzaldehyde (32). 3-(Chloromethyl)-4-methoxybenzaldehyde (**29**) (1.63 g, 8.8 mmol), 4-chlorophenol (1.23 ml, 12.5 mmol) and potassium carbonate (1.66 g, 12.0 mmol) are dissolved in DMF (40 ml) and stirred for 18 h. The reaction is diluted with ethyl acetate and washed with HCl 1 M and brine. The organic layer is dried over sodium sulfate, filtered and the solvent is removed under reduced pressure. The crude residue is purified by silica gel column chromatography (hexane/ethyl acetate = 8/1) to give the desired product **32** (1.98 g, 82 %) as a white solid. ¹H NMR (400 MHz, CDCl₃) δ 9.91 (s, 1 H), 8.01 (dd, *J* = 2.1, 1.0 Hz, 1 H), 7.87 (dd, *J* = 8.5, 2.2 Hz, 1 H), 7.25 (d, *J* = 7.7 Hz, 2 H), 7.03 (d, *J* = 8.5 Hz, 1 H), 6.98 – 6.90 (m, 2 H), 5.09 (s, 2 H), 3.96 (s, 3 H).

5.1.2.31. 1-(3-((4-Chlorophenoxy) methyl)-4-methoxyphenyl) ethan-1-one (33). Compound **32** (320 mg, 1.2 mmol) is dissolved in anhydrous THF (20 ml) and placed at 0 °C under nitrogen, then methyl magnesium bromide (3.0 M Et₂O, 600 μl, 1.8 mmol) is added dropwise. The reaction is stirred 20 min, then it is quenched with few drops of glacial acetic acid. The mixture is diluted with ethyl acetate and washed with HCl 1 M and brine. The organic layer is collected and dried over sodium sulfate, filtered and the solvent is removed under reduced pressure to give the intermediate secondary alcohol that is used without further purification. The crude material (341 mg, 1.2 mmol) is dissolved in toluene (20 ml) and cooled at 0 °C under nitrogen. A solution of trimethyl aluminium (2.0 M toluene, 200 ml, 0.4 mmol) is added dropwise. The mixture is allowed to warm to room temperature then cyclohexanone (700 μl, 6.8 mmol) is added and the reaction is stirred at reflux under nitrogen for 2 h. The reaction is quenched with NaHCO₃ saturated water solution and extracted with ethyl acetate. The organic layer is washed with HCl 1 M and brine then it is dried over sodium sulfate, filtered and the solvent is removed under reduced pressure. The crude residue is purified by silica gel column chromatography (petroleum ether/ethyl acetate = 10/3) to afford **32** (243 mg, 72 %) as a white solid. ¹H NMR (300 MHz, CDCl₃) δ 8.08 (d, *J* = 2.4 Hz, 1 H), 7.97 (dd, *J* = 8.7, 2.4 Hz, 1 H), 7.25 – 7.20 (m, 2 H), 7.00 – 6.89 (m, 3 H), 5.08 (s, 2 H), 3.93 (d, *J* = 1.7 Hz, 3 H), 2.56 (d, *J* = 1.7 Hz, 3 H).

5.1.2.32. *1-(3-((4-Chlorophenoxy)methyl)-4-methoxyphenyl)-4,4,4-trifluoro-3-(trifluoromethyl)butane-1,3-diol (34)*. Following general procedure B, starting from **33** (222 mg, 0.8 mmol) the product (petroleum ether/ethyl acetate = 8:1) **34** (268 mg, 73 %) is obtained as a white solid. $^1\text{H NMR}$ (400 MHz, CDCl_3) δ 7.46 (d, $J = 2.3$ Hz, 1 H), 7.37 – 7.21 (m, 3 H), 6.99 – 6.90 (m, 3 H), 6.29 (s, 1 H), 5.24 (d, $J = 11.5$ Hz, 1 H), 5.07 (s, 2 H), 3.89 (s, 3 H), 2.74 (t, $J = 2.3$ Hz, 1 H), 2.45 – 2.30 (m, 1 H), 2.17 (d, $J = 15.4$ Hz, 1 H). $^{13}\text{C NMR}$ (100 MHz, CDCl_3) δ 157.4, 157.3, 134.4, 129.5, 126.5, 126.1, 126.0, 125.9, 123.7 (q, $J = 286$ Hz), 122.8 (d, $J = 284$ Hz) 116.3, 110.8, 76.5 (m), 71.7, 65.2, 55.8, 36.5. HPLC-MS (ESI): calcd for $\text{C}_{19}\text{H}_{17}\text{ClF}_6\text{O}_4$: 458,07; found m/z : 457.16 [M-H].

5.1.2.33. *1-(Chloromethyl)-2-methoxybenzene (35)*. 1-(Hydroxymethyl)-2-methoxybenzene (1.52 g, 11.0 mmol) is added to stirred aqueous HCl (12 M, 10 ml) at room temperature. The mixture is stirred for 30 min, then diethyl ether is added. The layers are separated, and the organic layer is washed with aqueous NaHCO_3 . After drying over sodium sulfate, the solvent is removed under reduced pressure to furnish **35** (1.7 g, quant.) as a viscous oil that is used without further purification. Analytical data agree with those reported [46].

5.1.2.34. *1-(4-Fluorophenyl)-2-(2-methoxyphenyl)ethan-1-ol (36)*. Compound **35** (1.59 g, 10.1 mmol) is stirred with activated magnesium (450 mg, 18.5 mmol) in anhydrous THF (100 ml) at reflux under nitrogen atmosphere for 30 min. It is then cooled to room temperature and the solution is added *via* a cannula to a solution of 4-fluoro-benzaldehyde (3.30 g, 26.6 mmol) in THF (20 ml). The reaction is allowed to proceed for 30 min at 0 °C, then it is quenched with ammonium chloride and water. Following extraction with ethyl acetate, the organic layer is washed with NaHCO_3 , brine, dried over sodium sulfate and filtered. The solvent is removed under reduced pressure and the crude product is purified with silica gel column chromatography (hexane/DCM = 1/1) to afford **36** (340 mg, 14 %) as a white solid. $^1\text{H NMR}$ (400 MHz, CDCl_3) δ 7.37 – 7.28 (m, 2 H), 7.25 – 7.19 (m, 1 H), 7.02 (dtd, $J = 8.8, 6.5, 1.9$ Hz, 3 H), 6.89 (t, $J = 7.1$ Hz, 2 H), 4.95 (dd, $J = 8.5, 4.1$ Hz, 1 H), 3.85 (s, 3 H), 3.09 (dd, $J = 13.6, 4.2$ Hz, 1 H), 2.95 (dd, $J = 13.6, 8.5$ Hz, 1 H).

5.1.2.35. *1-(4-Fluorophenethyl)-2-methoxybenzene (37)*. Compound **36** (230 mg, 0.92 mmol) is stirred 30 min with aqueous HCl (12 M, 5 ml). The mixture is then extracted with diethyl ether and washed with brine. After removal of the solvent, the crude material is dissolved in acetic acid (20 ml) and zinc powder is added (265 mg, 4 mmol). The mixture is heated to reflux for 60 min, then cooled to room temperature and filtered over a pad of celite. After removal of the solvent under reduced pressure, the product is purified with silica gel column chromatography (hexane) to afford **37** (129 mg, 60 %) as colorless oil. $^1\text{H NMR}$ (300 MHz, CDCl_3) δ 7.13 (dddd, $J = 24.0, 18.4, 7.7, 1.7$ Hz, 4 H), 7.00 – 6.82 (m, 4 H), 3.82 (s, 3 H), 2.86 (m, 4 H).

5.1.2.36. *1-(3-(4-Fluorophenethyl)-4-methoxyphenyl)ethan-1-one (38)*. Compound **30** (129 mg, 0.57 mmol) is dissolved in DCM (8 ml) and cooled to 0 °C. Aluminium trichloride (150 mg, 1.14 mmol) and acetic anhydride (100 μl , 1.1 mmol) are added under nitrogen atmosphere and the reaction is stirred for 20 min, when it is quenched with water. The mixture is extracted with DCM, the organic layer washed with NaHCO_3 and brine. The solvent is removed under reduced pressure and the crude residue is purified with silica gel column chromatography (petroleum ether/DCM = 1/1) to afford compound **38** (105 mg, 68 %) as a white solid. $^1\text{H NMR}$ (300 MHz, CDCl_3) δ 7.84 (dd, $J = 8.6, 2.3$ Hz, 1 H), 7.70 (d, $J = 2.3$ Hz, 1 H), 7.17 – 7.07 (m, 2 H), 7.02 – 6.82 (m, 3 H), 3.88 (s, 3 H), 2.88 (dd, $J = 8.5, 5.0$ Hz, 4 H), 2.52 (s, 3 H).

5.1.2.37. *4,4,4-trifluoro-1-(3-(4-fluorophenethyl)-4-methoxyphenyl)-3-(trifluoromethyl)butane-1,3-diol (39)*. Following general procedure B,

starting from **38** (105 mg, 0.4 mmol) the product (petroleum ether/DCM = 4/1) **39** (143 mg, 81 %) is obtained as a white solid. $^1\text{H NMR}$ (300 MHz, CDCl_3) δ 7.22 – 7.03 (m, 3 H), 7.00 – 6.81 (m, 4 H), 6.21 (s, 1 H), 5.17 (d, $J = 11.6$ Hz, 1 H), 3.84 (s, 3 H), 2.96 – 2.77 (m, 4 H), 2.29 (ddd, $J = 15.5, 11.5, 2.0$ Hz, 1 H), 2.14 – 2.03 (m, 1 H). $^{13}\text{C NMR}$ (100 MHz, CDCl_3) δ 161.4 (d, $J = 242$ Hz), 158.0, 137.7, 133.9, 130.8, 130.0 (d, $J = 8$ Hz), 127.5, 124.7, 123.7 (q, $J = 286$ Hz), 122.8 (q, $J = 284$ Hz), 115.0 (d, $J = 21$ Hz), 110.6, 76.5 (m), 71.7, 55.6, 36.4, 35.3, 32.8. HPLC-MS (ESI): calcd for $\text{C}_{20}\text{H}_{19}\text{F}_7\text{O}_3$: 440.12; found m/z : 439.25 [M-H].

5.1.2.38. *4,4,4-Trifluoro-3-hydroxy-1-(4-methoxy-3-nitrophenyl)-3-(trifluoromethyl)butan-1-one (41)*. To a stirred solution of ketone **40** (547 mg, 2.8 mmol) at –60 °C in anhydrous THF (30 ml) under nitrogen atmosphere, LiHMDS (1.0 M solution in THF, 3.7 ml, 3.7 mmol) is added dropwise and stirred for 30 min. In a separate two neck flask, concentrated H_2SO_4 (15 ml) is warmed to 50 °C and connected through a cannula with the flask containing the ketone-enolate. An argon overpressure is applied to the flask containing sulfuric acid, while the flask at –60 °C is vented. HFA trihydrate (780 ml, 5.6 mmol) is added dropwise to the warm sulfuric acid and the gaseous HFA thus formed is delivered by the stream of argon to the cold enolate solution. When all the HFA has been delivered, the reaction is allowed to warm to room temperature. The reaction is quenched with glacial acetic acid (1.3 molar equivalent). The mixture is diluted with ethyl acetate and washed with water and brine. The organic layer is collected and dried over sodium sulfate, filtered and the solvent removed under reduced pressure. The crude product is purified by silica gel column chromatography (petroleum ether/ethyl acetate = 4/1) to afford the desired product **41** (320 mg, 31 %) as a white solid. $^1\text{H NMR}$ (300 MHz, CDCl_3) δ 8.47 (d, $J = 2.3$ Hz, 1 H), 8.20 (dd, $J = 8.9, 2.3$ Hz, 1 H), 7.30 – 7.20 (m, 1 H), 6.87 (s, 1 H), 4.11 (s, 3 H), 3.45 (s, 2 H).

5.1.2.39. *1-(3-Amino-4-methoxyphenyl)-4,4,4-trifluoro-3-(trifluoromethyl)butane-1,3-diol (42)*. Compound **41** (320 mg, 0.9 mmol) is dissolved in methanol (10 ml) and chilled at 0 °C. Sodium borohydride (50 mg, 1.33 mmol) is added. The reaction is stirred for 20 min then it is quenched with sodium bicarbonate. The mixture is diluted with water and extracted with ethyl acetate. The organic layer dried over sodium sulfate, filtered and the solvent is removed under reduced pressure. The crude residue is dissolved in a mixture of ethanol, water and acetic acid (7/1.5/1.5, 10 ml) and iron powder (430 mg, 7.7 mmol) is added. The reaction is stirred at room temperature for 3 h and then filtered on a pad of celite. The filtrate is evaporated to dryness and directly purified by silica gel column chromatography (petroleum ether/ethyl acetate = 1/1) to afford **42** (232 mg, 70 %) as a white solid. $^1\text{H NMR}$ (300 MHz, CD_3OD) δ 6.87 – 6.76 (m, 2 H), 6.69 (dd, $J = 8.2, 2.1$ Hz, 1 H), 5.03 (d, $J = 11.0$ Hz, 1 H), 3.84 (s, 3 H), 2.32 – 2.17 (m, 1 H), 2.08 (dd, $J = 15.3, 2.4$ Hz, 1 H).

5.1.2.40. *4-fluoro-N-(2-methoxy-5-(4,4,4-trifluoro-1,3-dihydroxy-3-(trifluoromethyl)butyl)phenyl)benzamide (43)*. Compound **36** (52 mg, 0.2 mmol) is dissolved in pyridine and cooled to 0 °C. 4-fluoro benzoyl chloride (30 μl , 0.25 mmol) is added and the mixture is stirred and allowed to room temperature over the course of 4 h. The mixture is poured over water and extracted three times with ethyl acetate, washed with HCl 1 M, water and brine. The organic layer is collected and dried over sodium sulfate. After removal of the solvent under reduced pressure, the crude product is purified by silica gel column chromatography (petroleum ether/ethyl acetate = 3/1) to afford **43** (30 mg, 82 %) as a white solid. $^1\text{H NMR}$ (400 MHz, $\text{DMSO}-d_6$) δ 9.53 (s, 1 H), 8.07 – 7.99 (m, 2 H), 7.77 (d, $J = 2.2$ Hz, 1 H), 7.40 – 7.31 (m, 2 H), 7.20 (dd, $J = 8.5, 2.2$ Hz, 1 H), 7.08 (d, $J = 8.5$ Hz, 1 H), 5.00 (d, $J = 9.9$ Hz, 1 H), 3.83 (s, 3 H), 2.23 (dd, $J = 15.2, 10.1$ Hz, 1 H), 2.15 – 2.07 (m, 1 H). $^{13}\text{C NMR}$ (100 MHz, $\text{DMSO}-d_6$) δ 164.1 (d, $J = 247$ Hz), 164.1, 151.1,

136.6, 131.0, 130.2 (d, $J = 9$ Hz), 126.6, 123.6 (q, $J = 289$ Hz), 123.1, 123.0 (q, $J = 286$ Hz) 122.0, 115.6, 115.4, 111.3, 75.7 (m), 67.9, 55.9, 37.7. HPLC-MS (ESI): calcd for $C_{19}H_{16}F_7NO_4$: 455.10; found m/z : 454.23 [M-H].

5.1.2.41. 1-(3-Amino-4-methoxyphenyl)ethan-1-one (44). Compound **33** (2.07 g, 10.6 mmol) is dissolved in ethanol (35 ml) and acetic acid (7 ml) then iron powder (5.91 g, 106.0 mmol) is added. The reaction is stirred at room temperature for 3 h then filtered over a pad of celite. The solvents are removed under reduced pressure and the crude product is directly subjected to silica gel column chromatography (petroleum ether/ethyl acetate = 4/1) to afford the product **44** (1.08 g, 62 %) as a brown solid. 1H NMR (300 MHz, DMSO- d_6) δ 7.25 – 7.19 (m, 2 H), 6.92 – 6.83 (m, 1 H), 4.93 (s, 2 H), 3.84 (s, 3 H), 2.44 (s, 3 H).

5.1.2.42. N-(5-acetyl-2-methoxyphenyl)-4-fluorobenzamide (45). Compound **44** (1.08 g, 6.51 mmol) is dissolved in pyridine and cooled to 0 °C. 4-Fluoro benzoyl chloride (920 ml, 7.78 mmol) is added and the mixture is stirred and allowed to warm to room temperature over the course of 4 h. The mixture is poured over water and extracted three times with ethyl acetate, washed with HCl 1 M, water and brine. The organic layer is collected and dried over sodium sulfate. After removal of the solvent under reduced pressure, the crude product is purified by silica gel column chromatography (petroleum ether/ethyl acetate = 3/1) to afford **45** (1.23 g, 66 %) as a white solid. 1H NMR (300 MHz, $CDCl_3$) δ 9.16 (d, $J = 2.2$ Hz, 1 H), 8.46 (s, 1 H), 7.98 – 7.87 (m, 2 H), 7.82 (dd, $J = 8.6, 2.2$ Hz, 1 H), 7.20 (t, $J = 8.6$ Hz, 2 H), 7.00 (d, $J = 8.7$ Hz, 1 H), 4.02 (s, 3 H), 2.63 (s, 3 H).

5.1.2.43. N-(5-acetyl-2-methoxyphenyl)-4-fluoro-N-methylbenzamide (46). Compound **38** (585 mg, 2.0 mmol) is dissolved in anhydrous THF (20 ml) at 0 °C and sodium hydride (60 mg, 2.4 mmol) and imidazole (15 mg, 0.2 mmol) are added. The reaction is stirred at 0 °C under nitrogen 20 min then methyl iodide (400 μ l, 6.1 mmol) is added dropwise. The reaction is stirred 2.5 h then it is quenched with few drops of glacial acetic acid. The mixture is diluted with Ethyl acetate and washed with brine. the organic layer is collected, and the solvent is removed under reduced pressure. The crude residue is purified by silica gel column chromatography (petroleum ether/ethyl acetate = 3/1) to afford the compound **46** (579 mg, 95 %) as a white solid. 1H NMR (300 MHz, $CDCl_3$) δ 7.80 (dd, $J = 8.6, 2.2$ Hz, 1 H), 7.72 (d, $J = 2.2$ Hz, 1 H), 7.30 (t, $J = 7.1$ Hz, 2 H), 6.82 (dt, $J = 8.6, 4.3$ Hz, 3 H), 3.78 (s, 3 H), 3.36 (s, 3 H), 2.49 (s, 3 H).

5.1.2.44. 4-Fluoro-N-(2-methoxy-5-(4,4,4-trifluoro-1,3-dihydroxy-3-(trifluoromethyl) butyl) phenyl)-N-methyl benzamide (47). Following general procedure B, starting from compound **46** (579 mg, 1.9 mmol), the product is purified by column chromatography (petroleum ether/ethyl acetate = 3:1) to give **47** (490 mg, 55 %) as a white solid. 1H NMR (300 MHz, $CDCl_3$) δ 7.14 (d, $J = 8.5$ Hz, 2 H), 6.93 (s, 1 H), 6.82 (d, $J = 8.3$ Hz, 2 H), 6.12 (s, 1 H), 5.08 (d, $J = 11.1$ Hz, 1 H), 3.80 (s, 3 H), 3.33 (s, 3 H), 2.22–1.75 (m, 2 H). ^{13}C NMR (100 MHz, $CD_3OD/CDCl_3$) δ 171.3, 163.2 (d, $J = 248$ Hz), 154.0, 136.1, 133.1, 132.0, 129.9, 129.8, 126.4, 126.3, 126.0, 125.6, 123.5 (q, $J = 286$ Hz), 122.6 (q, $J = 285$ Hz), 114.7, 114.4, 111.9, 76.2 (m), 69.4, 55.5, 36.8, 36.2. HPLC-MS (ESI): calcd for $C_{20}H_{18}F_7NO_4$: 469.11; found m/z : 468.17 [M-H].

5.1.2.45. 5-(Chloromethyl)-6-methoxy-3,4-dihydronaphthalen-1(2 H)-one (48). 6-Methoxy-3,4-dihydronaphthalen-1(2 H)-one (1.50 g, 8.5 mmol) and formaldehyde (0.34 g, 11.01 mmol) are dissolved in aqueous HCl (12 M, 8 ml). The mixture is stirred at room temperature for 2 h then diluted with water and washed with DCM. The organic layer is collected and dried over sodium sulfate, filtered and the solvent is removed under reduced pressure. The crude residue is purified by silica gel column chromatography (petroleum ether/ethyl acetate = 7/3) to

give the product **48** as a white solid (598 mg, 32 %). 1H NMR (300 MHz, $CDCl_3$) δ 8.06 (d, $J = 8.9$ Hz, 1 H), 6.88 – 6.73 (m, 1 H), 4.70 (s, 2 H), 3.89 (s, 3 H), 2.99 (t, $J = 6.1$ Hz, 2 H), 2.57 (t, $J = 6.5$ Hz, 2 H), 2.10 (d, $J = 6.5$ Hz, 2 H).

5.1.2.46. 5-((4-Fluorophenoxy)methyl)-6-methoxy-3,4-dihydronaphthalen-1(2 H)-one (49). Compound **48** (598 mg, 2.7 mmol), 4-fluoro phenol (431 mg, 3.5 mmol) and potassium carbonate (902 mg, 7.0 mmol) are dissolved in degassed DMF (30 ml). The mixture is stirred for 18 h, then is diluted with ethyl acetate and washed water and brine. The organic layer is collected and dried over sodium sulfate, filtered and the solvent is removed under reduced pressure. The crude residue is purified by silica gel column chromatography (petroleum ether/ $Et_2O = 10/3$) to give product **49** (298 mg, 37 %) as a white solid. 1H NMR (300 MHz, $CDCl_3$) δ 8.15 (d, $J = 8.8$ Hz, 1 H), 7.06 – 6.87 (m, 5 H), 5.11 (s, 2 H), 3.91 (s, 3 H), 3.01 (t, $J = 6.1$ Hz, 2 H), 2.61 (dd, $J = 7.4, 5.7$ Hz, 2 H), 2.12 (d, $J = 6.4$ Hz, 2 H).

5.1.2.47. 5-((4-Fluorophenoxy)methyl)-2-(1,1,1,3,3,3-hexafluoro-2-hydroxypropan-2-yl)-6-methoxy-1,2,3,4-tetrahydro naphthalen-1-ol (50). According to general procedure B, part i, starting from ketone **49** (147 mg, 0.5 mmol), product (petroleum ether/ $Et_2O = 10/2$) **50** (102 mg, 43 %) is obtained as a white solid. 1H NMR (300 MHz, $CDCl_3$) δ 8.19 (d, $J = 8.9$ Hz, 1 H), 7.08 – 6.89 (m, 5 H), 5.19 (d, $J = 10.5$ Hz, 1 H), 5.06 (d, $J = 10.5$ Hz, 1 H), 3.97 (s, 3 H), 3.29 (dt, $J = 17.1, 3.6$ Hz, 1 H), 3.20 – 3.08 (m, 1 H), 2.92 (ddd, $J = 17.2, 13.2, 4.0$ Hz, 1 H), 2.54 (dd, $J = 13.5, 3.9$ Hz, 1 H), 2.27 – 2.08 (m, 1 H). ^{13}C NMR (100 MHz, $CDCl_3$) δ 199.0, 163.2, 157.7 (d, $J = 238$ Hz), 154.9, 146.5, 131.9, 125.5, 123.5 (d, $J = 288$ Hz), 122.5 (d, $J = 285$ Hz) 122.0, 116.0 (d, $J = 23$ Hz), 115.9 (d, $J = 8$ Hz), 110.1, 79.21 (m), 61.1, 56.2, 45.0, 26.3, 24.3. HPLC-MS (ESI): calcd for $C_{21}H_{17}F_7O_4$: 466.10; found m/z : 465.12 [M-H].

5.1.2.48. Trans-5-((4-fluorophenoxy)methyl)-2-(1,1,1,3,3,3-hexafluoro-2-hydroxypropan-2-yl)-6-methoxy-1,2,3,4-tetrahydronaphthalen-1-ol (51). According to general procedure B, part ii, starting from **50** (82 mg, 0.17 mmol), product (petroleum ether/ $Et_2O = 10/3$) **51** (80 mg, quant.) is obtained as a white solid. 1H NMR (300 MHz, $CDCl_3$) δ 7.34 – 7.25 (m, 1 H), 7.12 – 6.81 (m, 5 H), 6.20 (s, 1 H), 5.09 (s, 2 H), 3.88 (s, 3 H), 3.20 (dt, $J = 17.9, 4.4$ Hz, 1 H), 2.87 (ddd, $J = 18.1, 11.1, 7.3$ Hz, 1 H), 2.40 (dd, $J = 19.2, 6.9$ Hz, 2 H), 2.32 – 2.13 (m, $J = 5.7$ Hz, 2 H). ^{13}C NMR (100 MHz, $CDCl_3$) δ 158.8, 157.5 (d, $J = 238$ Hz), 155.2, 155.1, 138.1, 131.8, 129.2, 124.0 (q, $J = 286$ Hz), 123.1 (q, $J = 287$ Hz), 122.5, 116.0 (d, $J = 14$ Hz), 115.8 (d, $J = 2$ Hz), 109.8, 79.9 (m), 70.1, 61.5, 56.0, 38.8, 26.1, 17.2. HPLC-MS (ESI): calcd for $C_{21}H_{19}F_7O_4$ [M-H]: 468.12; found m/z : 467.14 [M-H].

5.1.2.49. Tert-butyl dimethyl((6-(4,4,5,5-tetramethyl-1,3,2-dioxaborolan-2-yl) naphthalen-2-yl) oxy) silane (52). A mixture of compound **20** (340 mg, 1.0 mmol), bis(pinacolato)diboron (430 mg 1.7 mmol), Pd (Dppf) Cl_2 (37 mg, 0.05 mmol) and potassium acetate (1.0 g, 10.1 mmol) in 1,4-dioxane is heated at reflux for 6 h. After removal of the solvent under reduced pressure, the crude material is purified by silica gel column chromatography (petroleum ether/ $Et_2O = 10/2$), to obtain **52** (131 mg, 34 %) as a white solid. 1H NMR (400 MHz, $CDCl_3$) δ 8.29 (s, 1 H), 7.81 – 7.73 (m, 2 H), 7.67 (d, $J = 8.2$ Hz, 1 H), 7.17 (d, $J = 2.4$ Hz, 1 H), 7.06 (dd, $J = 8.8, 2.4$ Hz, 1 H), 1.38 (s, 12 H), 1.02 (s, 9 H), 0.25 (s, 6 H).

5.1.2.50. 1-(4-(6-((Tert-butyl)dimethylsilyl) oxy) naphthalen-2-yl)-3-(chloromethyl) phenyl) ethan-1-one (54). According to general procedure A, starting from compound **52** (247 mg, 0.6 mmol) and **53** (151 mg, 0.6 mmol), the product (hexane/ethyl acetate = 100/5) **54** (203 mg, 73 %) is obtained as a white solid. 1H NMR (400 MHz, $CDCl_3$) δ 8.18 (d, $J = 1.9$ Hz, 1 H), 7.98 (dd, $J = 8.1, 1.8$ Hz, 1 H), 7.85 – 7.67 (m, 4 H),

7.48 (dd, $J = 7.4, 2.1$ Hz, 2 H), 7.15 (dd, $J = 8.8, 2.4$ Hz, 1 H), 4.62 (s, 2 H), 2.68 (s, 3 H), 1.04 (s, 9 H), 0.28 (s, 6 H).

5.1.2.51. 1-(4-(6-((*Tert*-butyldimethylsilyl)oxy)naphthalen-2-yl)-3-((4-fluorophenoxy)methyl)phenyl)ethan-1-one (**55**). Compound **54** (198 mg, 0.5 mmol), 4-fluorophenol (158 mg, 1.4 mmol) and potassium carbonate (500 mg, 3.5 mmol) are dissolved in DMF and stirred for 16 h at room temperature. The mixture is diluted with diethyl ether and washed with water and brine. The solvent is removed under reduced pressure and the crude residue is purified by silica gel column chromatography (toluene/Et₂O = 10/1) to give product **54** (60 mg, 25 %) as a white solid. ¹H NMR (300 MHz, CDCl₃) δ 8.24 (d, $J = 1.8$ Hz, 1 H), 8.00 (d, $J = 1.9$ Hz, 1 H), 7.80–7.64 (m, 3 H), 7.53 (d, $J = 8.0$ Hz, 1 H), 7.49–7.40 (m, 1 H), 7.24–7.11 (m, 2 H), 6.99–6.85 (m, 2 H), 6.85–6.75 (m, 2 H), 4.97 (s, 2 H), 2.67 (s, 3 H), 0.91 (s, 9 H), 0.10 (s, 6 H).

5.1.2.52. 4,4,4-Trifluoro-1-(3-((4-fluorophenoxy)methyl)-4-(6-hydroxynaphthalen-2-yl)phenyl)-3-hydroxy-3-(trifluoromethyl)butan-1-one (**56**). To a solution of compound **55** (55 mg, 0.1 mmol) at –60 °C in anhydrous THF (10 ml) under nitrogen atmosphere, LiHMDS (1.0 M solution in THF, 130 ml) is added dropwise and stirred for 30 min. In a separate two neck flask, concentrated H₂SO₄ (15 ml) is warmed to 50 °C and connected through a cannula with the flask containing the ketone-enolate. An argon overpressure is applied to the flask containing sulfuric acid, while the flask at –60 °C is vented. HFA trihydrate (500 μl, 3.6 mmol) is added dropwise to the warm sulfuric acid and the gaseous HFA thus formed is delivered by the stream of argon to the cold enolate solution. When all the HFA has been delivered, the reaction is allowed to warm to room temperature. Tetrabutylammonium fluoride (TBAF, 1.0 M solution in THF, 200 μl, 0.2 mmol) is added to the reaction and the mixture is stirred at room temperature for 3 h. The mixture is diluted with ethyl acetate and washed with water and brine. The organic layer is collected and dried over sodium sulfate, filtered and the solvent is removed under reduced pressure. The crude product is purified by silica gel column chromatography (hexane/Et₂O = 10/5) to afford product **56** (35 mg, 58 %) as a white solid. ¹H NMR (300 MHz, CDCl₃) δ 8.26 (d, $J = 2.0$ Hz, 1 H), 8.02 (dd, $J = 8.1, 2.0$ Hz, 1 H), 7.82–7.68 (m, 3 H), 7.60 (d, $J = 8.1$ Hz, 1 H), 7.45 (dd, $J = 8.4, 1.8$ Hz, 1 H), 7.22–7.11 (m, 2 H), 7.01–6.87 (m, 2 H), 6.87–6.75 (m, 2 H), 5.00 (s, 2 H), 3.52 (s, 2 H).

5.1.2.53. 4,4,4-Trifluoro-1-(3-((4-fluorophenoxy)methyl)-4-(6-hydroxynaphthalen-2-yl)phenyl)-3-(trifluoromethyl)butane-1,3-diol (**57**). Compound **56** (35 mg, 0.1 mmol) is dissolved in methanol (5 ml) at 0 °C and sodium borohydride (10 mg, 0.2 mmol) is added. The mixture is stirred for 1 h, then the reaction is quenched with aqueous NaHCO₃. The mixture is diluted with ethyl acetate and washed with water and brine. The organic layer is collected and dried over sodium sulfate, filtered and the solvent is removed under reduced pressure. The crude product is purified by silica gel column chromatography (toluene/ethyl acetate = 10/1) to afford **57** (30 mg, 90 %) as a white solid. ¹H NMR (400 MHz, CDCl₃) δ 7.55–7.42 (m, 4 H), 7.30–7.19 (m, 2 H), 7.11–7.02 (m, 1 H), 6.95 (ddd, $J = 24.0, 9.1, 2.9$ Hz, 2 H), 6.72 (t, $J = 8.6$ Hz, 2 H), 6.59 (dd, $J = 9.1, 4.3$ Hz, 2 H), 6.13 (s, 1 H), 5.16 (d, $J = 11.4$ Hz, 1 H), 4.72 (s, 2 H), 2.30–2.19 (m, 1 H), 2.16 (s, 1 H), 2.08 (d, $J = 15.4$ Hz, 1 H). ¹³C NMR (100 MHz, CDCl₃) δ 157.6 (d, $J = 238$ Hz), 154.5, 154.5, 154.0, 142.8, 141.6, 135.1, 134.9, 134.0, 131.3, 130.2, 128.7, 128.1, 127.9, 126.7, 125.5, 123.7 (q, $J = 287$ Hz), 122.8 (q, $J = 282$ Hz), 118.6, 116.1 (d, $J = 1$ Hz), 116.0 (d, $J = 16$ Hz), 76.8 (m), 71.9, 68.8, 36.5. HPLC-MS (ESI): calcd for C₂₈H₂₁F₇O₄: 554.13; found m/z: 553.02 [M-H]⁺.

5.1.2.54. 1,1,1-Trifluoro-2-hydroxy-2-(trifluoromethyl)undecan-4-one (**58**). According to general procedure B, starting from nonan-2-one (**57**, 500 mg, 3.5 mmol) **58** (180 mg, 58 %) is obtained as a colorless oil. ¹H NMR (400 MHz, CDCl₃) δ 6.27 (s, 1 H), 4.24 (dd, $J = 10.1, 5.4$ Hz, 1 H), 2.28–1.84 (m, 4 H), 1.60 (d, $J = 1.0$ Hz, 1 H), 1.53 (dd, $J = 7.0, 6.2$ Hz,

2 H), 1.33–1.26 (m, 8 H), 0.97–0.85 (m, 3 H). ¹³C NMR (100 MHz, CDCl₃) δ 123.6 (q, $J = 286$ Hz), 122.9 (q, $J = 286$ Hz), 76.7 (m), 70.0, 38.8, 34.0, 31.8, 29.4, 29.2, 24.9, 22.7, 14.2. HPLC-MS (ESI): calcd for C₁₂H₂₀F₆O₂: 310.14; found m/z: 309.18 [M-H].

5.2. Molecular modeling

5.2.1. Docking studies

The structure of the macromolecular target was retrieved from the RCSB Protein Data Bank (www.rcsb.org, PDB ID 1FQ9). The PDB file was selected in agreement with a previous work [12]. 3D models of ligands were built using Avogadro 1.2.0, and geometry was optimized using the same software [47]. Target was prepared for the blind docking experiments, performed using AutoDock Vina (Molecular Graphics Laboratory, Department of Integrative Structural and Computational Biology, The Scripps Research Institute, CA, USA), using default parameters [35]. Prior to docking studies, FG2 was isolated from the structure (chain A) and all the other molecules were removed. Receptor search volume was set according to the grid parameters reported in the following. Grid center: x = 67.897, y = 25.5412, z = 120.184, size: 35 × 35 × 35 Å. The number of docking poses was set to 10, with other Vina parameters set as default. Residue numbering used in the PDB file was adopted. Output data, such as calculated binding energies and interaction patterns, were analyzed and scored using UCSF Chimera molecular viewer [48]. This software was also used to produce the artworks. Calculated binding energy values are expressed in kcal/mol and refer to the most favored predicted pose.

5.2.2. Molecular dynamics simulations

MD simulations were carried out using PlayMolecule (Acellera, Middlesex, UK) [49] starting from the output models of docking experiments. Ligands were prepared by running Parametrize function based on GAFF2 force field. Each complex was prepared for the simulation using ProteinPrepare and SystemBuilder functions, setting pH = 7.4, AMBER 14SB force field and default experiment parameters [50]. Consequently, N terminus of the protein (His16) was capped with an acetyl group and the side chain of Lys18 was reconstructed, while C terminus was modified to obtain the methyl amide of Ala144. MD simulations of 25 ns were carried out using SimpleRun, with default settings [36]. Each simulation run was performed in triplicate. Plotting of root mean-square deviation (RMSD) values of ligand heavy atoms over time was performed using Excel 15.31 (Microsoft, WA, USA).

5.2.3. Binding pose metadynamics

Enhanced sampling simulations were carried out using the binding pose metadynamics program, version 1.0, within the Schrödinger suite 2019–4. Protein-ligand complexes were energy-minimized using MacroModel 12.6 [51] by applying the OPLS3e force field [52]. During the minimization, the position of the heavy atoms of the protein backbone was restrained by applying a harmonic restraint of 100 kcal·mol⁻¹·Å⁻², and the convergence threshold was set to 0.05 kJ·mol⁻¹·Å⁻¹. The minimized complexes were then submitted to the binding pose metadynamics protocol. Each complex was solvated using the SPC water model, setting the system box dimensions to 10 Å × 10 Å × 10 Å. All the systems were neutralized by adding 11 Cl⁻ counter ions. Following a default short equilibration molecular dynamics, 10 well-tempered metadynamics simulations were performed for each protein-ligand complex. The RMSD of the ligand heavy atoms from the equilibrated starting pose was used as biasing collective variable. A gaussian bias with an initial height of 0.05 kcal·mol⁻¹ and a width of 0.02 Å was added every 1.0 ps, while the scaling factor of the bias height was set to 4. Each simulation lasted for 10 ns and the last 2 ns of each simulation were used to calculate the PoseScore, which accounts for the thermodynamically favored RMSD averaged over the 10 independent runs [37].

5.3. Surface plasmon resonance (SPR)

A BIAcore X-100 apparatus (BIAcore Inc., Piscataway, NJ, USA) was used to perform surface plasmon resonance analyses as previously reported [12]. The equilibrium (plateau) values of the SPR sensorgrams were used to build the binding isotherms (dose-response curves). Binding isotherm points were fitted with the Langmuir equation for monovalent binding to evaluate the mass surface dissociation constant, K_d , and the scaling parameter that relates the SPR signal with the extent of binding, as the free parameters of the fitting. The errors on these parameters were assigned as a result of the fitting algorithm (95 % confidence bounds). The best-fitting procedure was performed with the SigmaPlot 11.0 software package (Systat Software Inc.).

5.4. HSPG/FGF2/FGFR1 mediated cell-cell adhesion assay

Wild-type CHO-K1 cells were seeded in a 48-well plate at 1.3×10^5 cells/cm² and grown till a monolayer was formed. After 24 hours, CHO-K1 monolayers were washed with PBS. Then, A745-CHO-flg-1A-luc cells were resuspended in a solution prepared with 0.1 % gelatin from porcine skin (Sigma-Aldrich, Saint Louis, MO), 0.1 mg/ml CaCl₂, 0.1 mg/ml MgCl₂ in PBS and 5×10^4 cells were added in each well with or without 30 ng/ml of FGF2 in absence and presence of increasing concentration of the compounds under test dissolved in 0.5 % DMSO. After 2 hours of incubation at 37°C, during which CHO-K1 cells bound the ligand FGF2 that in turn bound the expressed surface FGFR1 in A745-CHO-flg-1A-luc cells, the plate was washed with PBS to remove unattached cells. The remaining attached cells were lysed with 50 µL of luciferase buffer/well (80 mM Na₂HPO₄, 9.3 mM NaH₂PO₄, 2 % Triton) for 30 minutes. After that, luciferase activity was quantified. All experiments were performed in triplicate.

5.5. Cell cultures

KMS-11 and KMS-11/BTZ cells were obtained from the Japanese Collection of Research Bioresources (JCRB, Osaka, Japan) cell bank, and U266 and OPM2 cells from the German Collection of Microorganisms and Cell Cultures (DSMZ, Braunschweig, Germany). All MM cell lines were maintained at low passage in RPMI1640 medium supplemented with 10 % heat inactivated FBS and 2.0 mM glutamine. CHO-K1, CHO-R1 and A745-CHO-flg-1A-luc cells were generated as previously described [53] and cultured in F-12 Nut Mix (Gibco) with 10 % FBS.

All cell lines were tested regularly for Mycoplasma negativity, and authenticated by PowerPlex Fusion System (Promega, Madison, USA).

5.6. Patient-derived multiple myeloma cells

Approval for these studies was obtained from the local Ethics Committee (protocol n. NP2694). Informed consent was obtained from all patients in accordance with the Declaration of Helsinki protocol. Primary CD138⁺ cells were obtained from freshly isolated multiple myeloma patients' BM using CD138⁺ microbeads selection, as reported in Roccaro et al. [54].

5.7. Western blot analysis

Cells were washed in cold PBS and homogenized in NP-40 lysis buffer (1 % NP-40, 20 mM Tris-HCl pH 8, 137 mM NaCl, 10 % glycerol, 2 mM EDTA, 1 mM sodium orthovanadate, 10 mg/ml aprotinin, 10 mg/ml leupeptin). Protein concentration in the supernatants was determined using the Bradford protein assay (Bio-Rad Laboratories). Phosphorylated FGFR3 was detected using rabbit anti-FGFR3 (phospho Y724) antibody (Abcam) and the Phospho-FGF receptor (Tyr653/654) antibody (Cell Signaling Technology, Danvers, MA, USA) was used to detect the phosphorylated forms of all four FGF receptors. Also, rabbit anti-human c-Myc (Cell Signaling Technology), rabbit anti-pH2AX (Cell

Signaling Technology) and rabbit anti-human cleaved caspase 3 (Cell Signaling Technology) antibodies was used to detect the level of c-Myc protein, DNA damage and apoptotic cell death, respectively. β-actin or GAPDH were used as loading controls (antibodies from Sigma-Aldrich, Saint Louis, MO). Chemiluminescent signal was acquired by ChemiDoc™ Imaging System (BioRad) and analyzed using the ImageJ software (<http://rsb.info.nih.gov/ij/>).

5.8. Viable cell counting

MM cell lines and patient-derived MM cells were cultured under appropriate conditions for 48 or 12 hours, respectively. Propidium iodide staining (Immunostep, Salamanca, SP, EU) was used to detect PI negative viable cells by flow cytometry. Absolute cell counts were obtained by the counting function of the MACSQuant® Analyzer (Miltenyi Biotec). IC₅₀ values are the mean of at least 2 experiments performed in triplicate.

5.9. Mitochondrial ROS detection

Mitochondrial (mt)ROS production was determined using the fluorescent probe Mitosox according to manufacturer's instructions. Mitosox positive cells were detected by cytofluorimetric analysis with MACSQuant® Analyzer (Miltenyi Biotec).

5.10. Subcutaneous MM human xenografts

Experiments were performed according to the Italian laws (D.L. 116/92 and following additions) that enforce the EU 86/109 Directive and were approved by the local animal ethics committee (OPBA, Organismo Preposto al Benessere degli Animali, Università degli Studi di Brescia, Italy, protocol n. PR389/2017).

Six- to eight-week-old female NOD/SCID mice (Envigo, Udine, Italy) were injected subcutaneously (s.c.) with KMS-11 cells (5×10^6 cells/mouse) in 200 µl of PBS. When tumors were palpable, mice were randomly assigned to receive treatment with NSC12 (7.5 mg/kg), compound 22 (7.5 mg/kg), compound 57 (7.5 mg/kg) or control/vehicle DMSO. Treatments were performed IP every other day. Tumor volumes were measured with calliper and calculated according to the formula $V = (D \times d^2)/2$, where D and d are the major and minor perpendicular tumor diameters, respectively. At the end of the experimental procedure, tumor nodules were excised, weighed, photographed and processed for histological analyses.

5.11. Histological analyses

Formalin-fixed, paraffin-embedded samples were sectioned at a thickness of 3 µm, dewaxed, hydrated, and processed for immunohistochemistry with rabbit anti-human phospho-FGF receptor (Tyr653/654) (Cell Signaling Technology), rabbit anti-human c-Myc (Cell Signaling Technology), rabbit anti-nitrotyrosine (Millipore), rabbit anti-γH2AX (Cell Signaling Technology), rabbit anti-human phospho-Histone H3 (Chemicon) or rabbit anti-human cleaved caspase 3 (Cell Signaling Technology) antibodies.

Sections were finally counterstained with Carazzi's hematoxylin before analysis by light microscopy.

5.12. In vivo toxicity

To assess the absence of in vivo toxicity of compound 29 and 57, whole blood and serum from treated animals were collected and analysed in terms of blood cell composition and biochemical parameters, respectively. Also, mice body weight was monitored during treatment.

5.13. Statistical analyses

Statistical analyses were performed using Prism 8 (GraphPad Software). Student t test for unpaired data (two-tailed) was used to test the probability of significant differences between two groups of samples. For more than two groups of samples, data were analyzed with a one-way ANOVA and corrected by the Bonferroni multiple comparison test. Tumor volume data were analyzed with a two-way analysis of variance and corrected by the Bonferroni test. Differences were considered significant when $P < 0.05$.

Funding

This work was supported by grants from Fondazione Cariplo (grant n. 2016-0570) to AG and from Associazione Italiana Ricerca sul Cancro to AG (AIRC grant IG 2023n. 28939), MP (AIRC grants IG 2016 n. 18943 and IG 2019 n. 23116), RR (AIRC grant IG 2019 n. 23151) and AMR (AIRC grant IG24689), ST was supported by Associazione Garda Vita (R. Tosoni) fellowship. GG was supported by Consorzio Interuniversitario per le Biotecnologie (CIB) short-term abroad fellowship and Guido Berlucci Foundation young researchers mobility programme. RR, MR and MP are grateful to Consorzio Interuniversitario per le Biotecnologie (CIB) for its support.

CRedit authorship contribution statement

Sara Taranto: Investigation, Data curation. **Marco Rusnati:** Investigation, Data curation. **Jessica Faletti:** Methodology, Investigation. **Edoardo Rocca:** Investigation, Methodology. **Giovanni Ribaud:** Methodology, Investigation. **Roberto Ronca:** Investigation, Funding acquisition, Data curation. **Giorgia Gazzaroli:** Methodology, Investigation. **Marco Mor:** Writing – review & editing, Supervision, Conceptualization. **Laura Scalvini:** Methodology, Investigation. **Marco Presta:** Writing – review & editing, Supervision, Funding acquisition, Conceptualization. **Giuseppe Marseglia:** Methodology, Investigation. **Silvia Rivara:** Writing – original draft, Supervision, Data curation, Conceptualization. **Alessandra Gianoncelli:** Methodology, Investigation. **Arianna Giacomini:** Writing – original draft, Supervision, Funding acquisition, Data curation, Conceptualization. **Federica Vacondio:** Methodology, Investigation. **Aldo Maria Roccaro:** Investigation, Funding acquisition. **Riccardo Castelli:** Investigation, Data curation. **Antonio Sacco:** Investigation.

Declaration of Competing Interest

The authors declare that they have no known competing financial interests or personal relationships that could have appeared to influence the work reported in this paper.

Data availability

Data will be made available on request.

Acknowledgements

This research benefits from the HPC (High Performance Computing) facility of the University of Parma, Italy (<http://www.hpc.unipr.it>).

Appendix A. Supporting information

Supplementary data associated with this article can be found in the online version at [doi:10.1016/j.phrs.2024.107291](https://doi.org/10.1016/j.phrs.2024.107291).

References

- [1] Y. Xie, N. Su, J. Yang, Q. Tan, S. Huang, M. Jin, Z. Ni, B. Zhang, D. Zhang, F. Luo, H. Chen, X. Sun, J.Q. Feng, H. Qi, L. Chen, FGF/FGFR signaling in health and disease, *Signal Transduct. Target Ther.* 5 (2020) 181, <https://doi.org/10.1038/s41392-020-00222-7>.
- [2] A. Giacomini, P. Chiodelli, S. Matarazzo, M. Rusnati, M. Presta, R. Ronca, Blocking the FGF/FGFR system as a "two-compartment" antiangiogenic/antitumor approach in cancer therapy, *Pharmacol. Res.* 107 (2016) 172–185, <https://doi.org/10.1016/j.phrs.2016.03.024>.
- [3] A.-M. Chioni, R.P. Groose, Biological significance and targeting of the FGFR axis in cancer, *Cancers* 13 (2021) 5681, <https://doi.org/10.3390/cancers13225681>.
- [4] N. Hallinan, S. Finn, S. Cuffe, S. Rafee, K. O'Byrne, K. Gately, Targeting the fibroblast growth factor receptor family in cancer, *Cancer Treat. Rev.* 46 (2016) 51–62, <https://doi.org/10.1016/j.ctrv.2016.03.015>.
- [5] H.R. Ferguson, M.P. Smith, C. Francavilla, Fibroblast growth factor receptors (FGFRs) and noncanonical partners in cancer signaling, *Cells* 10 (2021) 1201, <https://doi.org/10.3390/cells10051201>.
- [6] A.N. Brooks, E. Kilgour, P.D. Smith, Molecular pathways: fibroblast growth factor signaling: a new therapeutic opportunity in cancer, *Clin. Cancer Res.* 18 (2012) 1855–1862, <https://doi.org/10.1158/1078-0432.Ccr-11-0699>.
- [7] J. Zheng, W. Zhang, L. Li, Y. He, Y. Wei, Y. Dang, S. Nie, Z. Guo, Signaling pathway and small-molecule drug discovery of FGFR: a comprehensive review, *Front. Chem.* 10 (2022) 860985.
- [8] M. Presta, P. Chiodelli, A. Giacomini, M. Rusnati, R. Ronca, Fibroblast growth factors (FGFs) in cancer: FGF traps as a new therapeutic approach, *Pharmacol. Ther.* 179 (2017) 171–187, <https://doi.org/10.1016/j.pharmthera.2017.05.013>.
- [9] T.C. Harding, L. Long, S. Palencia, H. Zhang, A. Sadra, K. Hestir, N. Patil, A. Levin, A.W. Hsu, D. Charych, T. Brennan, J. Zanghi, R. Halenbeck, S.A. Marshall, M. Qin, S.K. Doberstein, D. Hollenbaugh, W.M. Kavanaugh, L.T. Williams, K.P. Baker, Blockade of nonhormonal fibroblast growth factors by FP-1039 inhibits growth of multiple types of cancer, *178ra39, Sci. Transl. Med.* 5 (2013), <https://doi.org/10.1126/scitranslmed.3005414>.
- [10] M. Camozzi, M. Rusnati, A. Bugatti, B. Bottazzi, A. Mantovani, A. Bastone, A. Inforzato, S. Vincenti, L. Bracci, D. Mastroianni, M. Presta, Identification of an antiangiogenic FGF2-binding site in the N terminus of the soluble pattern recognition receptor PTX3, *J. Biol. Chem.* 281 (2006) 22605–22613, <https://doi.org/10.1074/jbc.M601023200>.
- [11] R. Ronca, A. Giacomini, E. Di Salle, D. Coltrini, K. Pagano, L. Ragona, S. Matarazzo, S. Rezzola, D. Maiolo, R. Torrella, E. Moroni, R. Mazzieri, G. Escobar, M. Mor, G. Colombo, M. Presta, Long-Pentaxin 3 Derivative as a Small-Molecule FGF Trap for Cancer Therapy, *Cancer Cell* 28 (2015) 225–239, <https://doi.org/10.1016/j.ccell.2015.07.002>.
- [12] R. Castelli, A. Giacomini, M. Anselmi, N. Bozza, F. Vacondio, S. Rivara, S. Matarazzo, M. Presta, M. Mor, R. Ronca, Synthesis, structural elucidation, and biological evaluation of NSC12, an orally available fibroblast growth factor (FGF) ligand trap for the treatment of FGF-dependent lung tumors, *J. Med. Chem.* 59 (2016) 4651–4663, <https://doi.org/10.1021/acs.jmedchem.5b02021>.
- [13] R. Castelli, S. Taranto, L. Furiassi, N. Bozza, G. Marseglia, F. Ferlenghi, S. Rivara, M. Retini, A. Bedini, G. Spadoni, S. Matarazzo, R. Ronca, M. Presta, M. Mor, A. Giacomini, Chemical modification of NSC12 leads to a specific FGF-trap with antitumor activity in multiple myeloma, *Eur. J. Med. Chem.* 221 (2021) 113529, <https://doi.org/10.1016/j.ejmech.2021.113529>.
- [14] O. Rabal, J.A. Sánchez-Arias, M. Cuadrado-Tejedor, I. de Miguel, M. Pérez-González, C. García-Barroso, A. Ugarte, A. Estella-Hermoso de Mendoza, E. Sáez, M. Espelosin, S. Ursua, T. Haizhong, W. Wei, X. Musheng, A. García-Osta, J. Oyarzabal, Design, synthesis, biological evaluation and in vivo testing of dual phosphodiesterase 5 (PDE5) and histone deacetylase 6 (HDAC6)-selective inhibitors for the treatment of Alzheimer's disease, *Eur. J. Med. Chem.* 150 (2018) 506–524, <https://doi.org/10.1016/j.ejmech.2018.03.005>.
- [15] T.M. Razler, Y. Hsiao, F. Qian, R. Fu, R.K. Khan, W. Doubleday, A preparatively convenient ligand-free catalytic PEG 2000 Suzuki–Miyaura coupling, *J. Org. Chem.* 74 (2009) 1381–1384, <https://doi.org/10.1021/jo802277z>.
- [16] J.K. Whitesell, D. Reynolds, Resolution of chiral alcohols with mandelic acid, *J. Org. Chem.* 48 (1983) 3548–3551, <https://doi.org/10.1021/jo00168a035>.
- [17] The absolute stereochemistry has not been determined.
- [18] R.E. Mewshaw, R.J. Edsall, C. Yang, E.S. Manas, Z.B. Xu, R.A. Henderson, J. C. Keith, H.A. Harris, ER β ligands. 3. Exploiting two binding orientations of the 2-phenylanthralene scaffold to achieve ER β selectivity, *J. Med. Chem.* 48 (2005) 3953–3979, <https://doi.org/10.1021/jm058173s>.
- [19] M. Roberti, D. Pizzirani, M. Recanatini, D. Simoni, S. Grimaudo, A. Di Cristina, V. Abbadessa, N. Gebbia, M. Tolomeo, Identification of a terphenyl derivative that blocks the cell cycle in the G0–G1 phase and induces differentiation in leukemia cells, *J. Med. Chem.* 49 (2006) 3012–3018, <https://doi.org/10.1021/jm060253o>.
- [20] B.B. Jarvis, J.C. Saukaiis, Nucleophilic displacements on halogen atoms. II. Kinetic study of the reactions of α -halo sulfones with triphenylphosphine, *J. Am. Chem. Soc.* 95 (1973) 7708–7715, <https://doi.org/10.1021/ja00804a027>.
- [21] V.V. Grushin, W.J. Marshall, G.A. Halliday, F. Davidson, V.A. Petrov, Facile preparation and synthetic applications of $\text{LiCH}_2\text{C}(\text{CF}_3)_2\text{Oli}$, *J. Fluor. Chem.* 117 (2002) 121–129, [https://doi.org/10.1016/S0022-1139\(02\)00154-9](https://doi.org/10.1016/S0022-1139(02)00154-9).
- [22] D.S. Khachatryan, A.L. Razinov, A.V. Kolotaev, S.K. Belus, K.R. Matevosyan, Alkylation of NH, OH, and SH acids in the presence of potassium carbonate 1. Functionalization of chloromethyl group of alkoxy-substituted aromatic aldehydes, *Russ. Chem. Bull.* 64 (2015) 395–404.

- [23] E.J. Campbell, H. Zhou, S.T. Nguyen, Catalytic Meerwein–Ponndorf–Verley reduction by simple aluminum complexes, *Org. Lett.* 3 (2001) 2391–2393, <https://doi.org/10.1021/ol0162116>.
- [24] C.R. Graves, B.-S. Zeng, S.T. Nguyen, Efficient and selective Al-catalyzed alcohol oxidation via oppenauer chemistry, *J. Am. Chem. Soc.* 128 (2006) 12596–12597, <https://doi.org/10.1021/ja063842s>.
- [25] S. Amin, S.S. Hecht, D.J. Hoffman, Synthesis of angular ring methoxy-5-methylchrysenes and 5-methylchrysenols, *J. Org. Chem.* 46 (1981) 2394–2398, <https://doi.org/10.1021/jo00324a039>.
- [26] M.L. Di Vona, V. Rosnati, Zinc-promoted reactions. I. Mechanism of the Clemmensen reaction. Reduction of benzophenone in glacial acetic acid, *J. Org. Chem.* 56 (1991) 4269–4273, <https://doi.org/10.1021/jo00013a036>.
- [27] J. Oyamada, Z. Hou, Regioselective C-H Alkylation of anisoles with olefins catalyzed by cationic half-sandwich rare earth alkyl complexes, *Angew. Chem. Int. Ed.* 51 (2012) 12828–12832, <https://doi.org/10.1002/anie.201206233>.
- [28] P. Friedel, J.M. Crafts, Sur une nouvelle méthode générale de synthèse d'hydrocarbures, d'acétone, etc. *Compt. Rend.* 87 (1877) 1392.
- [29] M. Koura, T. Matsuda, A. Okuda, Y. Watanabe, Y. Yamaguchi, S. Kurobuchi, Y. Matsumoto, K. Shibuya, Design, synthesis and pharmacology of 1,1-bistrifluoromethylcarbinol derivatives as liver X receptor β -selective agonists, *Bioorg. Med. Chem. Lett.* 25 (2015) 2668–2674, <https://doi.org/10.1016/j.bmcl.2015.04.080>.
- [30] M.T. Bogert, L.P. Curtin, The relation between molecular structure and odor in trisubstituted benzenes. I. Derivatives of para-methoxy-acetophenone, *J. Am. Chem. Soc.* 45 (1923) 2161–2167.
- [31] J. Delobelle, M. Fétizon, Synthèses totales dans la série des diterpènes. III. Ether méthylique du nimbiol, *Bull. Soc. Chim. Fr.* (1961) 1900–1905.
- [32] Y. Jia, Y. Xu, R. Nie, F. Chen, Z. Zhu, J. Wang, H. Jing, Artificial photosynthesis of methanol from carbon dioxide and water via a Nile red-embedded TiO₂ photocathode, *J. Mater. Chem. A* 5 (2017) 5495–5501, <https://doi.org/10.1039/C6TA10231J>.
- [33] R. Richelda, D. Ronchetti, L. Baldini, L. Cro, L. Viggiano, R. Marzella, M. Rocchi, T. Otsuki, L. Lombardi, A.T. Maiolo, A. Neri, A novel chromosomal translocation t(4;14)(p16.3;q32) in multiple myeloma involves the fibroblast growth factor receptor 3 gene, *Blood* 90 (1997) 4062–4070, <https://doi.org/10.1182/blood.V90.10.4062>.
- [34] A. Bikfalvi, S. Klein, G. Pintucci, D.B. Rifkin, Biological roles of fibroblast growth factor-2, *Endocr. Rev.* 18 (1997) 26–45, <https://doi.org/10.1210/edrv.18.1.0292>.
- [35] O. Trott, A.J. Olson, AutoDock Vina: improving the speed and accuracy of docking with a new scoring function, efficient optimization, and multithreading, *J. Comput. Chem.* 31 (2010) 455–461, <https://doi.org/10.1002/jcc.21334>.
- [36] S. Doerr, M.J. Harvey, F. Noé, G. De Fabritiis, HTMD: high-throughput molecular dynamics for molecular discovery, *J. Chem. Theory Comput.* 12 (2016) 1845–1852, <https://doi.org/10.1021/acs.jctc.6b00049>.
- [37] A.J. Clark, P. Tiwary, K. Borrelli, S. Feng, E.B. Miller, R. Abel, R.A. Friesner, B. J. Berne, Prediction of protein–ligand binding poses via a combination of induced fit docking and metadynamics simulations, *J. Chem. Theory Comput.* 12 (2016) 2990–2998, <https://doi.org/10.1021/acs.jctc.6b00201>.
- [38] C. Richard, J.P. Liuzzo, D. Moscatelli, Fibroblast growth factor-2 can mediate cell attachment by linking receptors and heparan sulfate proteoglycans on neighboring cells, *J. Biol. Chem.* 270 (1995) 24188–24196, <https://doi.org/10.1074/jbc.270.41.24188>.
- [39] A. Giacomini, S. Taranto, S. Rezzola, S. Matarazzo, E. Grillo, M. Bugatti, A. Scotuzzi, J. Guerra, M. Di Trani, M. Presta, R. Ronca, Inhibition of the FGF/FGFR system induces apoptosis in lung cancer cells via c-Myc downregulation and oxidative stress, *Int. J. Mol. Sci.* 21 (2020) 9376, <https://doi.org/10.3390/ijms21249376>.
- [40] A. Sacco, C. Federico, A. Giacomini, C. Caprio, F. Maccarinelli, K. Todorci, V. Favasuli, A. Anastasia, M. Motta, D. Russo, G. Rossi, N. Bozza, R. Castelli, A. Neri, R. Ronca, C. Cattaneo, A. Tucci, M. Mor, M. Presta, A.M. Roccaro, Halting the FGF/FGFR axis leads to antitumor activity in Waldenström macroglobulinemia by silencing MYD88, *Blood* 137 (2021) 2495–2508, <https://doi.org/10.1182/blood.2020008414>.
- [41] R. Ronca, G.C. Ghedini, F. Maccarinelli, A. Sacco, S.L. Locatelli, E. Foglio, S. Taranto, E. Grillo, S. Matarazzo, R. Castelli, G. Paganini, V. Desantis, N. Cattaneo, A. Cattaneo, M. Mor, C. Ca, A. Stella, A.M. Belotti, Roccaro, M. Presta, Arianna Giacomini, F.G.F. Trapping, inhibits multiple myeloma growth through c-Myc degradation-induced mitochondrial oxidative stress, *Cancer Res* 80 (2020) 2340–2354, <https://doi.org/10.1158/0008-5472.CAN-19-2714>.
- [42] G. Bisping, R. Leo, D. Wenning, B. Dankbar, T. Padró, M. Kropff, C. Scheffold, M. Kröger, R.M. Mesters, W.E. Berdel, J. Kienast, Paracrine interactions of basic fibroblast growth factor and interleukin-6 in multiple myeloma, *Blood* 101 (2003) 2775–2783, <https://doi.org/10.1182/blood-2002-09-2907>.
- [43] D. Lesuisse, E. Albert, F. Bouchoux, E. Cérède, J.M. Lefrançois, M.O. Levif, S. Tessier, B. Tric, G. Teutsch, Biphenyls as surrogates of the steroidal backbone. Part 1: synthesis and estrogen receptor affinity of an original series of polysubstituted biphenyls, *Bioorg. Med. Chem. Lett.* 11 (2001) 1709–1712, [https://doi.org/10.1016/S0960-894X\(01\)00267-0](https://doi.org/10.1016/S0960-894X(01)00267-0).
- [44] S. Marchais-Oberwinkler, M. Wetzel, E. Ziegler, P. Kruchten, R. Werth, C. Henn, R. W. Hartmann, M. Frotscher, New drug-like hydroxyphenyl naphthol steroidomimetics as potent and selective 17 β -hydroxysteroid dehydrogenase type 1 inhibitors for the treatment of estrogen-dependent diseases, *J. Med. Chem.* 54 (2011) 534–547, <https://doi.org/10.1021/jml1009082>.
- [45] X. Morelli, R. Bourgeois, P. Roche, Chemical and structural lessons from recent successes in protein–protein interaction inhibition (2P2I), *Curr. Opin. Chem. Biol.* 15 (2011) 475–481, <https://doi.org/10.1016/j.cbpa.2011.05.024>.
- [46] E.A. Standley, T.F. Jamison, Simplifying nickel(0) catalysis: an air-stable nickel precatalyst for the internally selective benzylation of terminal alkenes, *J. Am. Chem. Soc.* 135 (2013) 1585–1592, <https://doi.org/10.1021/ja3116718>.
- [47] M.D. Hanwell, D.E. Curtis, D.C. Lonie, T. Vandermeersch, E. Zurek, G.R. Hutchison, Avogadro: an advanced semantic chemical editor, visualization, and analysis platform, *J. Cheminform.* 4 (2012) 17, <https://doi.org/10.1186/1758-2946-4-17>.
- [48] E.F. Pettersen, T.D. Goddard, C.C. Huang, G.S. Couch, D.M. Greenblatt, E.C. Meng, T.E. Ferrin, UCSF Chimera—a visualization system for exploratory research and analysis, *J. Comput. Chem.* 25 (2004) 1605–1612, <https://doi.org/10.1002/jcc.20084>.
- [49] R. Galvelis, S. Doerr, J.M. Damas, M.J. Harvey, G. De Fabritiis, A scalable molecular force field parameterization method based on density functional theory and quantum-level machine learning, *J. Chem. Inf. Model.* 59 (2019) 3485–3493, <https://doi.org/10.1021/acs.jcim.9b00439>.
- [50] G. Martínez-Rosell, T. Giorgino, G. De Fabritiis, PlayMolecule proteinprepare: a web application for protein preparation for molecular dynamics simulations, *J. Chem. Inf. Model.* 57 (2017) 1511–1516, <https://doi.org/10.1021/acs.jcim.7b00190>.
- [51] MacroModel version 12.6 Schrödinger suite 2019-4, Schrödinger LLC, 2019.
- [52] E. Harder, W. Damm, J. Maple, C. Wu, M. Reboul, J.Y. Xiang, L. Wang, D. Lupyan, M.K. Dahlgren, J.L. Knight, J.W. Kaus, D.S. Cerutti, G. Krilov, W.L. Jorgensen, R. Abel, R.A. Friesner, OPLS3: a force field providing broad coverage of drug-like small molecules and proteins, *J. Chem. Theory Comput.* 12 (2016) 281–296, <https://doi.org/10.1021/acs.jctc.5b00864>.
- [53] D. Leali, M. Belleri, C. Urbinati, D. Coltrini, P. Oreste, G. Zoppetti, D. Ribatti, M. Rusnati, M. Presta, Fibroblast growth factor-2 antagonist activity and angiostatic capacity of sulfated Escherichia coli K5 polysaccharide derivatives, *J. Biol. Chem.* 276 (2001) 37900–37908, <https://doi.org/10.1074/jbc.M105163200>.
- [54] A.M. Roccaro, Y. Mishima, A. Sacco, M. Moschetta, Y.-T. Tai, J. Shi, Y. Zhang, M. R. Reagan, D. Huynh, Y. Kawano, I. Sahin, M. Chiarini, S. Manier, M. Cea, Y. Aljawai, S. Glavey, E. Morgan, C. Pan, F. Michor, P. Cardarelli, M. Kuhne, I. M. Ghobrial, CXCR4 Regulates extra-medullary myeloma through epithelial-mesenchymal-transition-like transcriptional activation, *Cell Rep.* 12 (2015) 622–635, <https://doi.org/10.1016/j.celrep.2015.06.059>.